Applied Catalysis B: Environmental 224 (2018) 518–532

Contents lists available at ScienceDirect

Applied Catalysis B: Environmental

journal homepage: www.elsevier.com/locate/apcatb

Review

Unique role of Mössbauer spectroscopy in assessing structural features of heterogeneous catalysts

Xuning Li[a,b,c,d], Kaiyue Zhu[a,c], Jifeng Pang[a], Ming Tian[a], Jiayi Liu[a,b,c], Alexandre I. Rykov[a,b], Mingyuan Zheng[a], Xiaodong Wang[a], Xuefeng Zhu[a], Yanqiang Huang[a], Bin Liu[d], Junhu Wang[a,b,*], Weishen Yang[a], Tao Zhang[a,b,*]

[a] State Key Laboratory of Catalysis, Dalian Institute of Chemical Physics, Chinese Academy of Sciences, Dalian 116023, China
[b] Mössbauer Effect Data Center, Dalian Institute of Chemical Physics, Chinese Academy of Sciences, Dalian 116023, China
[c] University of Chinese Academy of Sciences, Beijing 100049, China
[d] School of Chemical and Biomedical Engineering, Nanyang Technological University, 62 Nanyang Drive, Singapore 637459, Singapore

ARTICLE INFO

Keywords:
Mössbauer spectroscopy
Catalytic reactions
Electrocatalysis
Fischer–Tropsch Synthesis
Mechanism investigation

ABSTRACT

Their wide availability in nature, low cost, high reactivity, and low toxicity make Fe-based catalysts versatile in various catalysis fields, including photocatalysis, Fenton-like reaction, electrocatalysis, Li-ion batteries (LIBs), Fischer–Tropsch synthesis (FTS), biomass conversion, N_2O decomposition and etc. Mössbauer spectroscopy, a powerful technique that is able to give account of structural features for all iron species taking part in the catalysis process, is considered to be a crucial technique for determining catalyst phase, identifying active site, and investigating correlations between catalytic behavior and the coordination structure of catalysts, which are highly desirable for clarifying the catalytic mechanisms. Each kind of Fe-based materials could be functionalized in the most suitable catalysis field, wherever Mössbauer technique may play a unique role. For instance, Fe-N-C based materials are extensively investigated as electrocatalysts for oxygen reduction reaction and Mössbauer spectroscopy application in this field has been utilized to identify the chemical nature of the active site on the Fe-N-C catalyst. Iron carbides are considered as the most active phase for FTS and Mössbauer technique is widely applied in determining the chemical phase of catalysts. Fe-based silicates, phosphates or polyanionic compounds are recognized as promising cathode materials for LIBs, for which Mössbauer technique has been mainly applied for tracking of the oxidation state and coordination environment change of Fe between charged and discharged states of the batteries. Similar phenomena can also be found in other catalysis fields. To give a clear understanding of which field is most suitable for a certain Fe-based catalyst and the best role of the Mössbauer technique in a certain catalysis field associated with the investigation of the mechanism, in this review, the recent advances of applying Mössbauer technique in catalysis are thoroughly summarized, including results from environmental catalysis and energy catalysis. Remarkable cases of study are highlighted and brief insight into applying Mössbauer technique for various Fe-based materials in their special catalysis field is presented. Finally, the trends for future potential applications of Mössbauer technique are discussed.

1. Introduction

Mössbauer spectroscopy, concerning the emission of γ-rays from exited nuclei and the absorption of these γ-rays by other nuclei of the same element, offers a powerful technique for the investigation of materials through measuring the hyperfine interactions arising from coupling the nuclear moments and electric and magnetic fields acting on the atomic nucleus. Isomer shift (δ; nomenclature for reporting Mössbauer Data from http://www.mossbauer.info/nomenclature.html; arises from Coulomb interaction between the nucleus and the s-electrons), quadrupole splitting (Δ; arises from interaction of the electric quadrupole moment of the nucleus with an electric field gradient) and magnetic hyperfine field (*B*; arises from interaction between the nuclear magnetic dipole moment and the magnetic field at the nucleus) are three main parameters in a Mössbauer spectrum, which gives information not only about the electron spin configuration and oxidation state, but also on the molecular symmetry and some clues about the magnetic structure involving the probe atom in a material under investigation [1]. Since 1959, Mössbauer spectroscopy has gradually become a routine method for catalysis characterizations. The further

* Corresponding authors at: Mössbauer Effect Data Center, Dalian Institute of Chemical Physics, Chinese Academy of Sciences, Dalian 116023, China.
E-mail addresses: wangjh@dicp.ac.cn (J. Wang), taozhang@dicp.ac.cn (T. Zhang).

http://dx.doi.org/10.1016/j.apcatb.2017.11.004
Received 2 August 2017; Received in revised form 2 November 2017; Accepted 3 November 2017
Available online 03 November 2017
0926-3373/ © 2017 Elsevier B.V. All rights reserved.

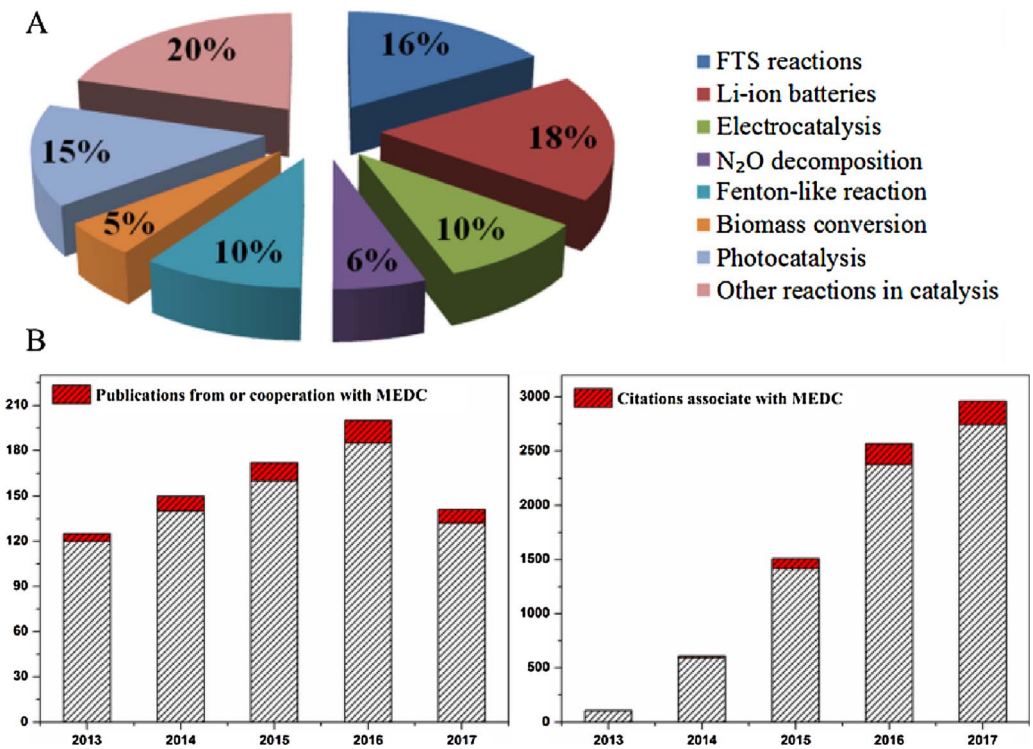

Fig. 1. (A) Number of articles from the years 2012–2017 on Mössbauer spectroscopy devoted to catalysis; (B) Publications and citations recorded by "Web of Science", returned by using the topic search criterion "Mössbauer" and "Cataly*" for the years 2013 through 2017.

development of its *in-situ* application capability makes Mössbauer technique unique for uncovering the "black box" of catalysis [2]. Over the past five years, Mössbauer technique has been extensively applied for the characterization of catalysts in various application fields such as photocatalysis [3–8], Fenton-like reaction [9–14], electrocatalysis [15–20], Li-ion batteries (LIBs) [21–27], Fischer–Tropsch synthesis (FTS) [28–35], biomass conversion [36–41], N_2O decomposition [42–48] and etc. (Fig. 1**A**). More than six hundred publications have ever been published and the citation numbers have been exponentially increased for years (Fig. 1**B**), revealing the fast development on applying Mössbauer technique in catalysis.

The majority of Mössbauer spectroscopy investigations dealt with elements of iron (Fe) and tin (Sn). Investigations of other elements, such as iridium (Ir), platinum (Pt), ruthenium (Ru), or gold (Au), are limited in numbers although fruitful [2]. The applications of Mössbauer technique in catalysis research are mainly focused on: (1) identification of the active sites or active phases for the catalysis processes; (2) investigation of the correlations between the structure of catalysts and their catalytic performance; and (3) characterization of catalysts during activation and deactivation of the reaction under *ex-situ* (or *in-situ*) conditions.

The applications of Mössbauer spectroscopy in catalysis and its theoretical principles were previously summarized [1,2,49], including an article we published in *Advances in Catalysis* two years ago. These reviews mainly focused on the physical principle of Mössbauer spectroscopy instead of in its applications in catalysis. In addition, the cognition of which field is most suitable for a certain Fe-based catalyst and the acme role of Mössbauer technique in different catalysis field are still ambiguous. Considering the rapid development of Mössbauer technique in various catalysis fields over the past 5 years, this review mainly focuses on the application of Mössbauer technique for the investigation of: (1) the impact of Fe doping TiO_2 to improve its photocatalytic performance; (2) the redox cycles and active sites of Fenton-like catalysts; (3) the active site of Fe-N-C and NiFe based materials as electrocatalysts; (4) the oxidation state and environment change of Fe in Fe-based silicates, phosphates and polyanionic compounds between charge and discharge states of LIBs; (5) the phase transformation of iron carbides as catalysts during or after FTS; (6) the crystallographic sites and structure of hexaaluminates as aerospace catalysts; and (7) the presence of Fe species for biomass conversion. Remarkable cases of study are highlighted and brief insights regarding the application of the Mössbauer technique for various Fe-based materials in their special catalysis field is pointed out. Finally, the potential future trends for the applications of Mössbauer technique are discussed.

2. Applications of the Mössbauer technique in environmental catalysis

2.1. Photocatalysis

2.1.1. Fe doped TiO_2

Photocatalysis offers a promising way to cope with both the growing environmental and energy problems. The most widely investigated photocatalyst is TiO_2, a cheap and non-toxic semiconductor sensitive to ultraviolet irradiation. However, the energy required for activating TiO_2 is very high due to its wide band gap [50–52]. Fe is widely used as a dopant to TiO_2, as it may act as electron traps and thus can narrow the band gap [53–55]. In addition, Fe is one of the few elements, which offer the opportunity for probing the local electronic structure of doped TiO_2 by Mössbauer spectroscopy.

Bajnóczi et al. reported Fe^{III}-doped TiO_2 prepared by the sol–gel technique (S samples) or flame hydrolysis (F samples) as heterogeneous photocatalysts [55]. Small but significant differences were also seen in the Mössbauer parameters of the F and S samples (δ = 0.40 mm/s, Δ = 0.70 mm/s for F; and δ = 0.30 mm/s, Δ = 0.90 mm/s for S). These data, together with the results of X-ray photoelectron spectroscopy (XPS) and extended X-ray absorption fine structure (EXAFS), indicate that the varied geometry around Fe^{III} systematically within the S-series is most probably the reason for the photocatalytic activity passed through a maximum with the increasing Fe^{III} concentration. W.Q. Li et al. further studied the impact of Fe doping on the electronic structure of rutile TiO_2 based on density functional theory (DFT) calculations [7]. The calculated Mössbauer signatures were found to be consistent with the available experimental data reported in the

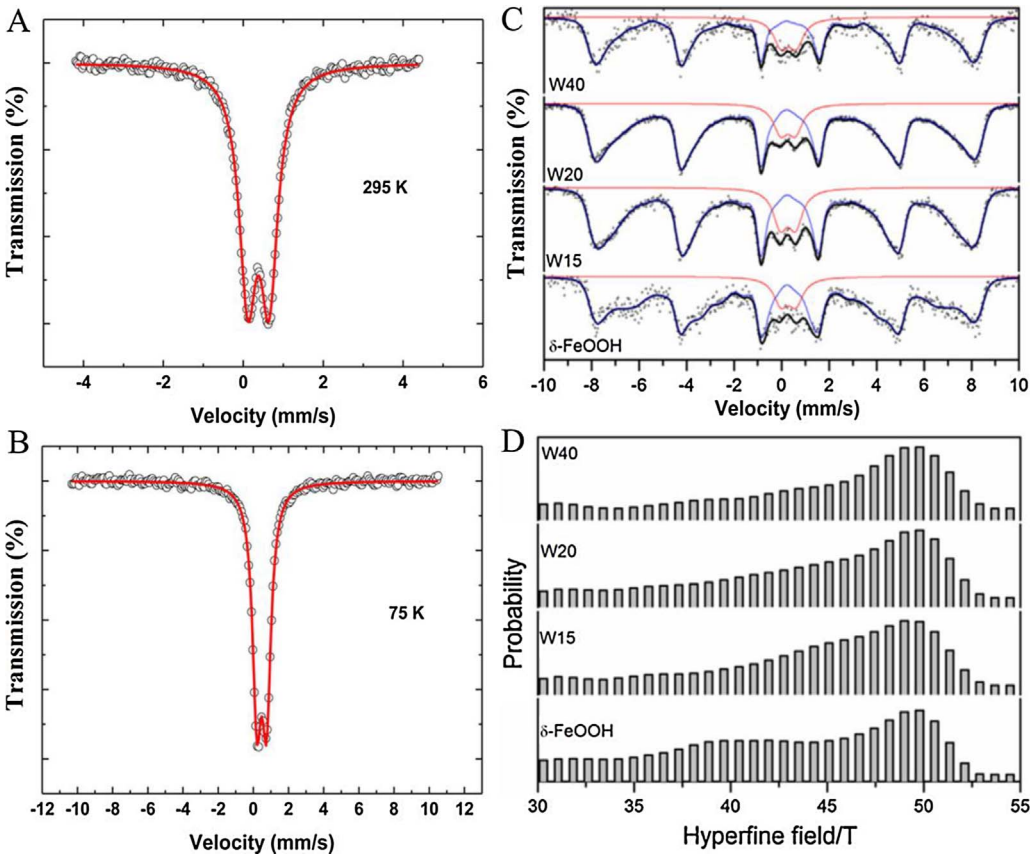

Fig. 2. ^{57}Fe Mössbauer spectra of 5% Fe^{3+} doped TiO_2 recorded at (A) 295 and (B) 75 K. (C) RT Mössbauer spectra and (D) hyperfine field distribution of Fe^{3+} in δ-FeOOH (the composites were labeled according to the W content).
Source: Reproduced with permission from Refs [3,5].

scientific literature. In addition, the δ value is rather close to the reference structures, and this is consistent with the calculated charge of Fe dopants with similar configuration to that in the pure oxides. These results proved that Fe doping could introduce mid-gap states and thus lower the band gap of TiO_2.

In the work of Andriamiadamanana et al. [3], Mössbauer spectroscopy was used to confirm the successful incorporation of up to 7.7% of Fe^{3+} into the TiO_2 crystal. The iron-doped nanocrystalline TiO_2 particles were synthesized by a novel room-temperature approach. The room temperature (RT) Mössbauer spectrum (Fig. 2**A**) is composed of a doublet, the hyperfine parameters of which give characteristic of Fe^{3+} in a high-spin configuration. The values of δ (0.38 mm/s) relative to alpha-Fe and Δ (0.53 mm/s) are typical for Fe^{3+} in a FeO_6-type octahedral site. The Mössbauer spectrum was found unchanged at liquid-nitrogen temperature (Fig. 2**B**). The best photocatalytic performance was obtained with 1 wt.% Fe-doped TiO_2. Recently, iron modified titanium–hafnium binary oxides were prepared by Tsoncheva et al. and Mössbauer technique was applied to reveal the co-existence of substituted $Fe_xTi_{1-x}O_2$ oxide and well crystallized α-Fe_2O_3 particles [56]. RT Mössbauer spectra of the iron modifications were fitted with two doublets and one sextet components. The doublet with Δ value about 1.21–1.28 mm/s and 0.70–0.78 mm/s was assigned to $Fe_xTi_{1-x}O_2$ and smaller α-Fe_2O_3 particles, respectively. The changes in the proportion of doublet and sextet components indicated that the incorporation of hafnium with small amount promotes the formation of $Fe_xTi_{1-x}O_2$, and Fe^{3+} ions substitute predominantly Ti^{4+}. The related catalytic properties and the percentage of various iron species were found to be regulated by hafnium incorporated in the lattice of TiO_2. In addition, results from the Mössbauer measurements revealed that the formation of $Fe_xTi_{1-x}O_2$ increased the dispersion of hematite particles. Mössbauer technique was performed in the recent work from Magdziarz et al. [57]. The results indicate that the studied photocatalysts contain only Fe^{3+} form dominantly in the tetrahedral coordination. The iron with aggregated hematite forms were formed in the photodeposition while an isolated Fe^{3+} oxide species were obtained in the sonodeposition (SPD). Therefore, the best performance for the oxidation of benzyl alcohol was obtained by the photocatalyst prepared by SPD.

In our group, a series of Fe-Sn codoped TiO_2 with different Fe concentrations (0.1–1.0 at.%) were prepared through a chemical solution method [58,59]. The dopant iron was found to preferably substitute the unsaturated coordination Ti ions. ^{57}Fe Mössbauer results revealed that Fe^{3+} ions tended to occupy the tetrahedrally coordinated site, especially in light doping level (≤1 at.%). As the Fe^{3+} dopant amount increased, it began to occupy the octahedral sites. The photocatalytic activity of Sn-Fe-0.1 (Fe/Ti = 0.1 at.%, Sn/Ti = 2.0 at.%) was found to be 5-fold of P25 and 2-fold of undoped TiO_2, indicating that the maximum synergistic effect in Fe-Sn codoped TiO_2 could be achieved by adjusting the concentration of oxygen vacancies as well as the ratio of tetrahedrally coordinated Ti^{4+} and Fe^{3+}.

2.1.2. Hybrid heterostructures of iron oxides

Constructing heterojunction provides a promising approach to improve the performance of iron oxide based photocatalysts [6,60–66]. Lima et al. recently prepared a series of δ-FeOOH/WO_3·H_2O heterojunctions with various WO_3 contents as photocatalysts [5]. Mössbauer spectra (Fig. 2**C, D**) were collected to explore the iron distribution in the δ-FeOOH. The Mössbauer spectra were analyzed with magnetic hyperfine field distribution method due to inhomogeneous particle size distribution of δ-FeOOH. The sextet and doublet components were assigned to octahedral Fe site in δ-FeOOH and superparamagnetism Fe^{3+} in small particles of δ-FeOOH, respectively. The Δ was found to increase proportionally with the content of W, demonstrating that the high distortion of Fe environment in the δ-FeOOH was most probably due to its strong interaction with WO_3 particles. In addition, the finely dispersed δ-FeOOH nanoparticles in W40 (40 wt.% of tungsten) were confirmed from the higher relative ratio of the Fe^{3+} doublet. The

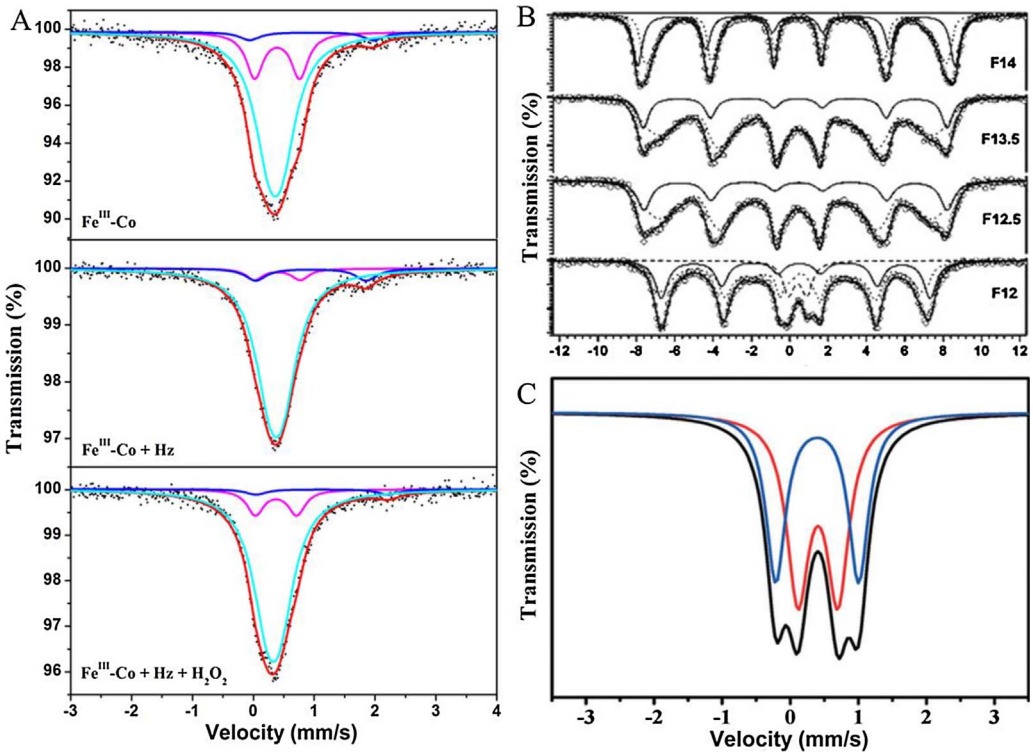

Fig. 3. (A) RT Mössbauer spectra of Fe^{III}-Co PBA proceeded in different reaction system. (B) 20 K Mössbauer spectra of the δ-FeOOH samples. (C) RT Mössbauer spectrum of MIL-53(Fe).
Source: Reproduced with permission from Refs [9,12,79].

results proved that the efficient separation of electrons and holes due to the formed heterojunctions in δ-FeOOH/WO_3 is the main origin for the high photocatalytic activity.

In the work performed by Tiago et al. [6], considering the magnetic relaxation, the Mössbauer spectra for hybrid nanocomposite of α-Fe_2O_3 and highly hydrophilic carbon dots (HCD) were analyzed with a hyperfine field of 51.9, 51.0 and 49.4 T. A linear temperature dependence of the magnetic hyperfine field was found to associate with the size of different α-Fe_2O_3 particles. Although the Δ distribution profile was distinguishable from that of the pure α-Fe_2O_3, it could be also ascribed to the existence of small sized Fe_2O_3 particles with superparamagnetic relaxation. Results of this work are important for the design of novel photocatalytic heterojunctions using iron oxides or HCD. The results of Mössbauer measurements in a recent work from Silva et al. indicate that magnetite could be partially converted into hematite during the heat treatment, which was the main active phase in the photocatalysts [64].

In our recent work [67], Mössbauer techniques were applied to investigate the coordination environments of Fe in visible light active iron oxide-titania nanocomposites. The fitted narrow and wide doublets were assigned to the tetrahedral (A-site) and octahedral (B-site) Fe^{III}, respectively. The photocatalytic performances of all prepared catalysts were found improved due to the accelerated separation of the photo-induced electron and hole pairs.

2.2. Fenton-like reaction

2.2.1. Investigate the redox cycles of Fe species

Fenton or Fenton-like processes, as one crucial technique of advanced oxidation processes (AOPs), has attracted extensive attention due to its simplicity, high efficiency and environmental friendliness [68–70]. Reactive oxygen species (HO·, HO_2·, and SO_4·$^-$ etc.) generated during the Fenton-like process could be highly efficient for decomposing nearly all organic pollutants rapidly [71,72]. Accelerating the redox cycles of Fe^{III} to Fe^{II} and understanding the heterogeneous Fenton reaction mechanism were considered as two main research hotspots to design heterogeneous Fenton catalysts with excellent activity as well as high durability [73,74]. ^{57}Fe Mössbauer spectroscopy, which is powerful to determine the spin and oxidation state as well as give insight into the coordination environment of Fe species in catalysts, was considered as an ideal technique to investigate the redox cycles of Fe in Fenton-like catalyst.

The further breakthrough of Fenton chemistry was largely hindered by the limited understanding of the reaction mechanism. In addition, the relationship between the efficiency of active radical generation and the structure of catalyst during the Fenton reaction are still unclear. For instance, by applying Mössbauer technique, Purceno et al. observed that the Fe^{II} was oxidized after Fenton process [75]. However, Yang et al. and Wang et al. reported the opposite phenomenon, where the reduction of Fe^{III} was observed after Fenton reaction and concluded that the reduction of Fe^{III} to Fe^{II} as the main factor for the long-term stability of the catalysts [73,76]. During the past two years, a series of progressed for investigating the mechanism of Fenton-like reaction have been made by our group using the capability of the Mössbauer technique to determine the coordination environment, spin and oxidation state of Fe species [77–79].

For instance, Prussian blue/TiO_2 (PB/TiO_2) nanocomposites as heterogeneous photo-Fenton catalysts were developed to accelerate the recovery of Fe^{II} for the removal of various organic pollutants. The Mössbauer results demonstrated that the excited electrons from TiO_2 with UV irradiation could accelerate the reduction of low spin Fe^{III} to Fe^{II} in PB and then lead to a better catalytic performance [77]. In the other work from our group, for in-depth study of the mechanism of heterogeneous Fenton reaction, Fe-Co Prussian blue analogues (PBAs) were developed as the novel photo-Fenton catalysts. Mössbauer spectroscopy was applied to explore the redox circulation of the Fe species under different simulative photo-Fenton processes. The accelerated reduction of Fe^{III} to Fe^{II} was proved to be crucial for the enhanced catalytic performance with the assistance of either low pH or visible light irradiation. In addition, the existence of abundant vacancies and highly dispersed water coordinated Fe sites in Fe-Co PBAs were proposed as the main factor for their excellent photo-Fenton activities [78].

To further study the reaction pathway of active Fe species during the Fe-Co PBA catalyzed Fenton-like process, hydrazine (Hz) was

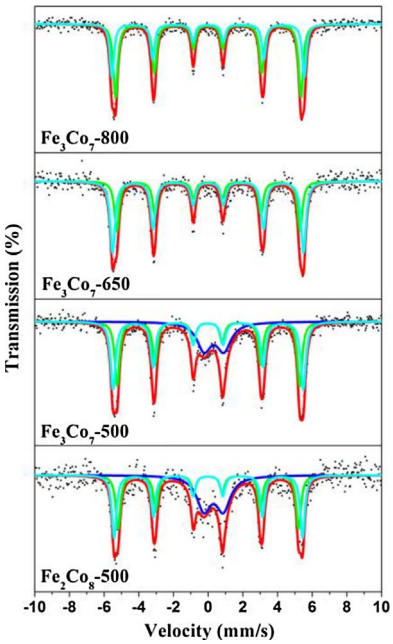

Fig. 4. Room temperature ^{57}Fe Mössbauer spectra of Fe_xCo_y@C nanocages.
Source: Reproduced with permission from Ref. [81].

applied to enhance the catalytic performance [79]. The Mössbauer spectra of Fe^{III}-Co PBA from different reaction systems were measured to explore the changes of the coordination environments of active Fe species during the Fenton-like process (Fig. 3**A**). The cyan and magenta doublets were assigned to six nitrogen coordinated Fe^{III} in $[Fe(CN)_6]^{3-}$ or $[Fe(CN)_5(Hz)]^{2-}$ (defined as: FeN_6) and five nitrogen and one water coordinated Fe^{III} in $[Fe(CN)_5(H_2O)]^{2-}$ (defined as: $(H_2O)FeN_5$), respectively. When both Hz and H_2O_2 were present in the reaction system, the content of Fe^{III} in FeN_6 was found to decrease with the increase of Fe^{III} in $(H_2O)FeN_5$. The results indicate that the reaction of H_2O_2 with $[Fe(CN)_5(Hz)]^{2-}$ most likely occurs during the Fenton-like process. Combining the XPS and Mössbauer results, the Hz coordinated Fe site (H_2NH_2N-Fe), evolved from the water coordinated Fe site (H_2O-Fe), was identified as a more active site which largely increased the catalytic performance.

2.2.2. Identify the active site of Fenton-like catalyst

The other main application of Mössbauer technique in Fenton chemistry is to identify the active site of Fenton-like catalyst. For instance, in the work of Pinto et al. [9], Mössbauer technique was applied to better understand the distribution of iron in δ-FeOOH samples. As shown in Fig. 3**B**, due to the particle size distribution, the spectra were fitted with a distributed magnetic hyperfine field for B-site Fe in δ-FeOOH. The RT Mössbauer parameters revealed a markedly lower *B* than that for the bulk δ-FeOOH (50.8 T for A-site and 53 T for B-site) due to superparamagnetic relaxation effects. The δ of 0.49-0.51 mm/s indicates that the Fe^{3+} is located only on the B-site in δ-FeOOH, which is most probably the main active site for the Fenton-like activity. For goethite (Gt; α-FeOOH), after dithionite treatment [80], the RT Mössbauer spectra present an increase in the central doublet, indicating increase of the percentage of small sized goethite particles. In addition, an adjustment of the sextet was found after dithionite treatment, suggesting the presence of reduced iron phase such as magnetite. The created Fe^{II} in the samples with the treatment of dithionite was proved as the main active site and largely increased the Fenton activity. Boron was also reported as a promoter to increase the Fenton activity of α-FeOOH (Gt-B) [14]. The Mössbauer spectrum of pure α-FeOOH was fitted with the superposition of two doublets, due to the superparamagnetic relaxation of the small-size Gt particles. Due to the excess of negative charges, B in Gt-B could cause a partial dihydroxylation which would increase in δ (0.37–0.39 mm/s) and Δ (0.04–0.99 mm/s). The Mössbauer results suggest that boron is capable to interact with surface iron and thus cause some crystalline defects in Gt. The presence of boron on the surface of iron oxide would be beneficial for the reduction of Fe^{III} to Fe^{II} and thus facilitate the electron transfer process, leading to the enhancement of the Fenton-like activity.

Besides goethite, iron oxides, zero-valent iron and Fe-containing metal-organic framework (MOFs) have been also widely investigated as Fenton-like catalysts. For instance, Coelho et al. reported Fe_2O_3/mesoporous silica (Fe-MS) as Fenton-like catalysts and characterized the samples by Mössbauer spectroscopy [11]. Mössbauer results reveal that the relative content for the superparamagnetic Fe^{3+} in Fe3-MS (prepared from $FeCl_3$) is higher than that in Fe2-MS (prepared from $FeCl_2$), indicating the better dispersion of iron on the silica matrix in Fe3-MS. These small clusters of iron oxides embedded into the flexible pore walls of mesoporous silica could efficiently participate in the reversible Fe^{III}-Fe^{II} redox process, which is the main factor for the higher activity of a Fenton-like system.

In the work done by Sun et al. [12], Mössbauer spectroscopy measurements gave a further insight into the oxidation state and the coordination environment of Fe in MIL-53 (MIL stands for Materials from Institut Lavoisier) and Fe(BDC)(DMF,F) as Fenton-like catalysts. Mössbauer spectra of MIL-53(Fe) (Fig. 3**C**) were fitted with two doublets assigned to Fe^{III}-OH (blue) and Fe^{III}-OH (red), respectively. Mössbauer results of Fe(BDC)(DMF,F) evidenced the existence of 20.8% high-spin state Fe^{II}, which was considered responsible for its higher Fenton activity.

The catalytic mechanism of sulfate radical ($SO_4\cdot^-$) based Fenton-like reaction, which to some extent could overcome the drawbacks of Fenton-like process using H_2O_2 as oxidizing agent [72], also deserves further investigation. In our recent research, porous $Fe_xCo_{3-x}O_4$ nanocages were prepared and applied as Fenton-like catalysts for peroxymonosulfate (PMS) activation [82]. The Mössbauer spectra of $Fe_{0.8}Co_{2.2}O_4$ before and after the Fenton-like reaction were recorded to study the role of Fe for the activation of PMS. Negligible changes observed after the reaction suggests that Fe in $Fe_xCo_{3-x}O_4$ nanocages was probably not the main factor for the high activity. Mössbauer spectroscopy was also applied to determine the oxidation state and coordination environment of Fe ions in nitrogen-doped graphene encapsulated Fe_xCo_y bimetallic (Fe_xCo_y@C) as Fenton-like catalysts (Fig. 4). The spectra were fitted with two sextets that could be assigned to the Fe_3Co_7 alloy with different chemical environments and/or crystallite sizes. Mössbauer spectra of Fe_3Co_7@C-500 and Fe_2Co_8@C-500 reveal the admixture of more than 20% of Fe_2O_3. The oxidation of the surface of the catalyst was demonstrated as the main reason for the lower Fenton-like activity [81].

3. Applications of the Mössbauer technique in electrocatalysis

3.1. Fe-N-C based materials

Fuel cells (FCs) provide a clean and efficient technology to convert chemical energy into electrical energy. However, the requirement of platinum as catalysts for the oxygen reduction reaction (ORR), makes FCs currently cost-prohibitive [83,84]. Since 1964, following the discovery of Co phthalocyanines as ORR catalysts [85], non-precious metal (NPM) Fe/Co-N based catalysts have attracted much attention due to the high activity and stability [86–89]. However, the lack of understanding on the ORR-active sites largely inhibited the advancements towards enhancing the activity of ORR catalysts. Till now, two models as the active sites were proposed. One model involves the metal particle encapsulated by the carbon shell; however, it does not take the requirement of nitrogen into consideration [90,91]. The other model proposed a porphyrin-like FeN_4 (or FeN_{2+2}) structure, however, the active species in most of reported the NPM catalysts are still unknown

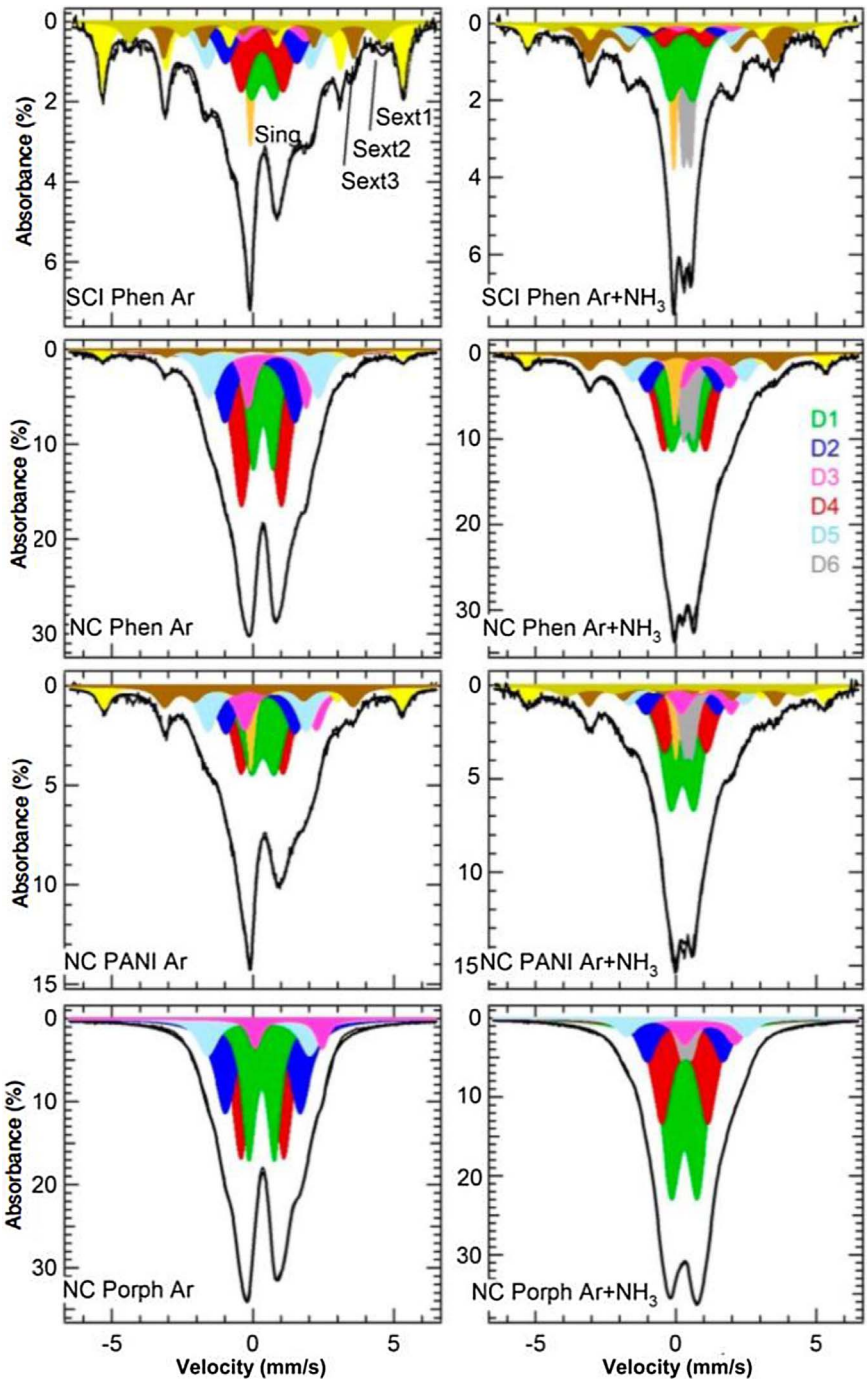

Fig. 5. Mössbauer spectra of the catalysts after the first heat treatment in Ar (left) and after the second heat treatment in NH_3 (right).
Source: Reproduced with permission from Ref. [15].

[92]. Because Mössbauer spectroscopy can distinguish various Fe-sites with similar structure in different spin and/or oxidation states, it is especially well suitable for analyzing Fe-N based ORR catalysts. Recently, a number of progressive research steps have been reported to identify the active site of ORR catalysts via applying Mössbauer technique.

Lefèvre et al. reported microporous carbon supported iron as ORR catalysts. The Fe cations coordinated with pyridinic N within the micropores of the graphitic sheet interstices were considered as the main active sites [17]. To clarify the mechanism for the enhanced ORR activity of these catalysts, Mössbauer spectroscopy was applied in a recent work from U.I. Kramm et al. [15]. One singlet, three sextets, and up to six doublets were used to fit the Mössbauer spectra (Fig. 5). The results demonstrated that among all FeN_4-like species, only D1 (FeN_4/C) and D3 (N-FeN_{2+2}/C) sites were active for ORR. In the work performed by Zhu et al. [93], o,m,p-phenylenediamine was used as the nitrogen precursor to tailor the Fe-N structures in the ORR catalysts containing FeS and Fe_3C phases. The δ values obtained from Mössbauer spectra were observed to increase with increasing the ligand bond length, indicating that the ORR activity is linear with the Fe-N bond length. From these observations, the authors identified the active sites in ORR catalysts with six-coordinate (FeN_6, [Fe^{III} (porphyrin)(pyridine)$_2$]).

In the work conducted by Zitolo et al. [95], a serie of Fe-N-C materials synthesized through the ammonia or argon pyrolysis exhibit similar Mössbauer spectra, revealing the same Fe-centered moieties in these ORR catalysts. By combining a quantitative analysis of the X-ray absorption near-edge structure (XANES) spectra with Mössbauer spectra, two porphyrinic FeN_4 architectures with different O_2

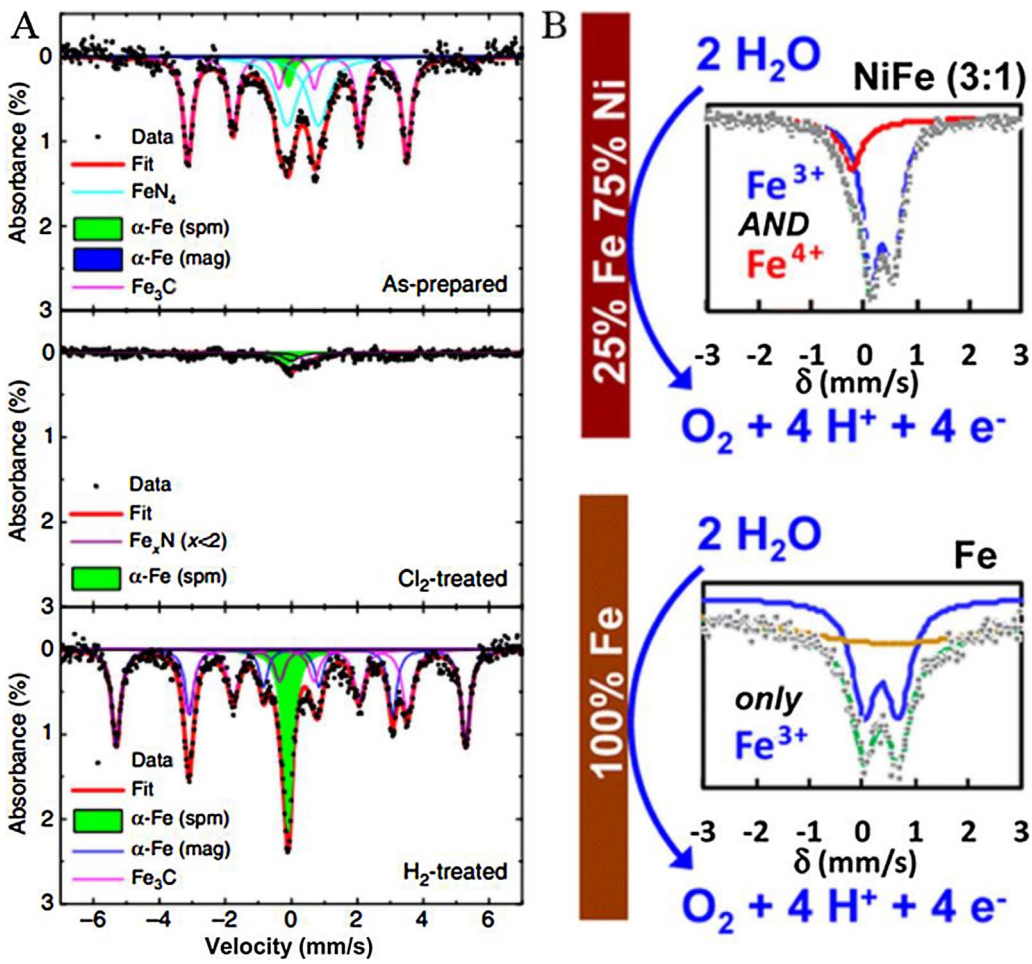

Fig. 6. (A) Mössbauer spectra and peak fitting of as-prepared, Cl_2-treated, and H_2-treated catalysts at 300 K. (B) Mössbauer spectra of NiFe and Fe-based OER catalysts under active OER condition.
Source: Reproduced with permission from Refs [16,94].

adsorption modes were identified. The electrochemical study demonstrates that such moieties catalyzed the four-electron reduction of O_2 to water.

The most recent breakthrough for identifying the active site of ORR catalysts through the application of Mössbauer spectroscopy was reported by Varnell et al. [16]. A reproducible deactivation and reactivation of the Fe-N based ORR catalysts were achieved via a respective high-temperature Cl_2 and H_2 treatments. The Mössbauer spectrum of the fresh catalyst (Fig. 6**A**) shows FeN_4 species, α-Fe and Fe_3C in the form of both superparamagnetic and magnetically split species. After high-temperature Cl_2 treatment, the Mössbauer spectrum (Fig. 6**A**) displays superparamagnetic α-Fe and a small amount of Fe_xN, with a largely decreased peak area as compared to the H_2-treated catalysts. The Mössbauer spectrum of H_2-treated catalyst reveals the only existence of α-Fe and contributions from Fe_3C. Noticeably, no signature of any Fe-N species could be found after H_2-treatement, which suggests that these sites are not essential for the ORR activity. Furthermore, the authors proposed that the reduced Fe species, protected by N-doped carbon, are the main active species for ORR.

Till now, the structure of the active site in Fe-N-C remains still elusive. This is due to not only the high requirement of specific spectroscopic techniques to explore the non-crystallographic ordering of the metal atoms, but also the simultaneous presence in most Fe-N-C catalysts along with other metal-based phases prevented recording the spectroscopic fingerprint of ORR-active sites. Therefore, the novel strategies for the preparation of Fe-N-C catalysts without metal-based phases, including iron based single-atom catalysts, as well as the development of *in-situ* Mössbauer technique are highly desired for the further insight of the active sites in Fe-N-C based materials.

3.2. NiFe based materials

The oxygen evolution reaction (OER), a process to produce molecular oxygen with assistance of either electricity or sunlight, poses one of the main bottlenecks in many energy conversion and storage devices, such as rechargeable metal air batteries, electricity or solar-driven water splitting for hydrogen generation [96–98]. NiFe-based materials have emerged as the most promising electrocatalysts toward OER and have been extensively investigated [94,97–101]. Mössbauer spectroscopy has been widely applied to gain insight into the role of Fe in these catalysts.

Recently, operando *in-situ* Mössbauer measurements in an electrochemical cell were carried out to probe the NiFe and Fe oxyhydroxide electrocatalysts under OER conditions by Chen et al. [94]. The Mössbauer spectra of the Ni:Fe (3:1) oxyhydroxide and hydrous Fe oxide catalysts collected under active OER condition are shown in Fig. 6**B**. Fe^{4+} species (the singlet; $\delta = -0.27$ mm/s), accounting for up to 21% of the total Fe, were detected in the NiFe oxyhydroxide during steady-state water oxidation process. In contrast, no Fe^{4+} species could be detected using the hydrous Fe oxide as catalyst. Although the observed Fe^{4+} species may not be kinetically competent for serving as the active site for OER, the discovery has important implications for understanding the role of Fe in NiFe-based catalysts for OER. By preparing a series of $NiFe/NiFeO_x$ core-shell OER catalysts, Zhu et al. [101] observed that the composition of $NiFe/NiFeO_x$ significantly influenced the OER activity. Mössbauer results reveal that all samples contain superparamagnetic Fe^{3+}, crystalline and amorphous Fe^0. Combined with high-resolution transmission electron microscopy (HRTEM), the crystalline and amorphous Fe^0 were located in the core of the catalysts, while the superparamagnetic Fe^{3+} was in the shell of the catalyst.

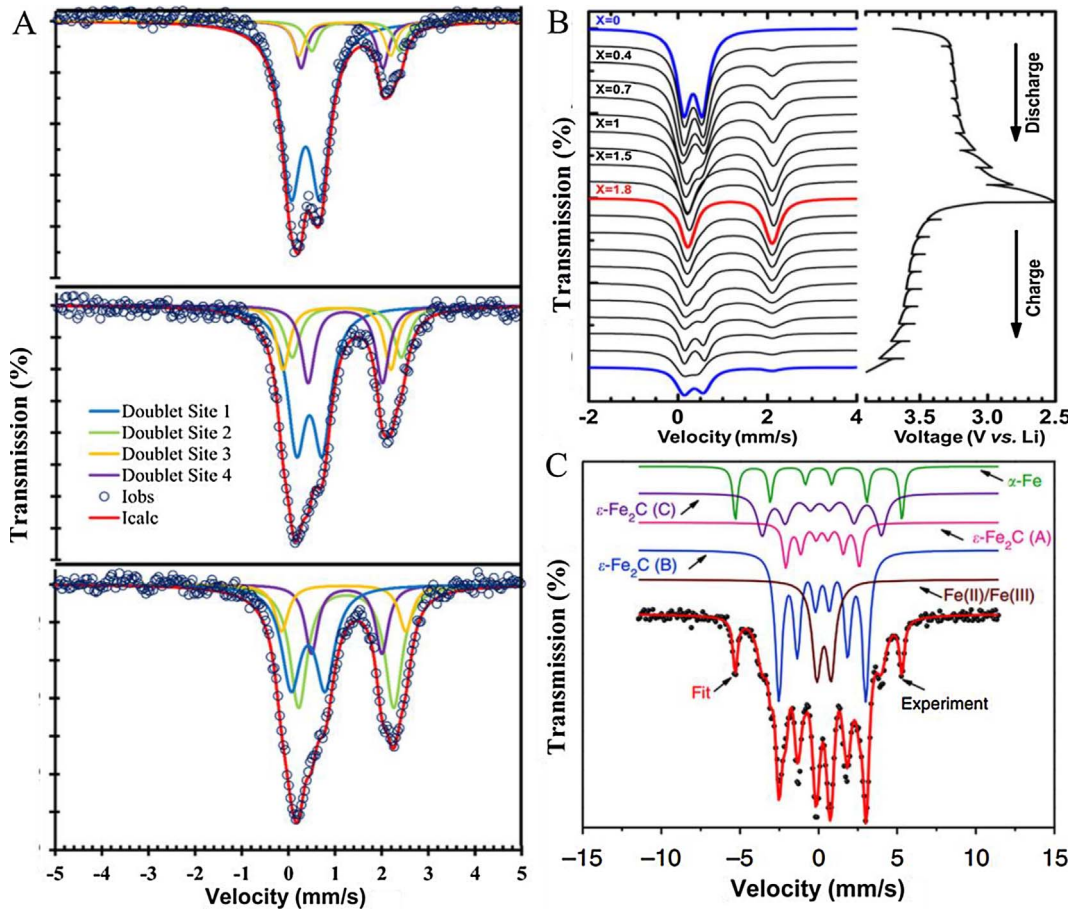

Fig. 7. (A) Mössbauer spectra of the $Li_xFe(H_2O)_2[BP_2O_8]\cdot H_2O$ cathode at various state-of-charge (SOC) charged to 4.0 V discharged to 3.0 V and discharged to 2.0 V. (B) Operando room temperature Mössbauer spectra of $Fe_2(C_2O_4)_3\cdot 4H_2O$ recorded during the electrochemical process at C/10 rate together with the voltage composition curve. (C) Mössbauer spectra of the highly reactive rapidly quenched skeletal iron (RQ Fe).
Source: Reproduced with permission from Refs [111,116,125].

Results of this work indicate that the metal core in the core-shell structure is facile for electron transport and thus extends the active sites to the surface of the catalyst, which is the main reason for the enhanced OER performance. In addition, Mössbauer spectroscopy was used to demonstrate the incorporation of Fe^{3+} into the β-$Ni(OH)_2$ lattice [102]. If Fe^{3+} is fully doped into the β-$Ni(OH)_2$ lattice, the OER activity increases directly with the content of Fe^{3+}. Besides, Zhu et al. made clever use of Mössbauer spectroscopy to prove the importance of the ordering of the layered structure in Fe-doped $LiNiO_2$ toward OER [103]. They found the full width at half maximum (FWHM) of the doublet for Fe^{3+} ions increased with increase of the iron amount, indicating a distribution of local environments around the iron ions and the loss of the layered structure. The importance of the layered structure to OER was further demenstrated by the density functional theory (DFT) calculations.

3.3. Spinel oxides

As a result of their various properties, spinel compounds have attracted lots of research interests in a wide range of applications including electrocatalysis for ORR and OER [104–106]. The composition effects as well as the cationic distribution effects were considered as the main factor affecting the electrocatalytic performance [107]. In our recent work [108], Mössbauer technique was applied to investigate the structure-function correlations between the ORR/OER activity and the cationic distribution in $Mn_xFe_{1.8-x}Co_{1.2}O_4$ spinel oxides. Results indicate that the octahedral-site Mn^{III}/Mn^{IV} content was directly correlated with the oxygen reduction/evolution reactions (ORR/OER) activity.

4. Applications of the Mössbauer technique in Li-ion batteries

Rechargeable Li-ion batteries (LIBs) are regarded as a promising technology for electric vehicles. The discovery of new materials with better performance and a clear insight into the intercalation electrode materials are both critical for ensuring a leap forward of LIBs [109,110]. Fe-based silicates, phosphates or polyanionic compounds as promising cathode materials for LIBs have been widely investigated, wherever Mössbauer technique was usually applied for tracking the oxidation state and environment change of Fe between charge and discharge states of the batteries [22–25,27,111–124].

4.1. Fe-based phosphates

Since 1997, double phosphates ($LiMPO_4$, M = Mn, Co, Fe, Ni) with an olivine structure have been recognized as promising alternative cathode materials for LIBs [126]. Recently, Abarca et al. reported a series of $Li_{1+x}Ti_{2-x}Fe_x(PO_4)_3$/C nanocomposites as electrodes for LIBs and Mössbauer spectroscopy was applied to give insight into the electrochemical lithium insertion mechanism [117]. The original compound, characterized by a doublet with δ value of 0.353 mm/s, confirmed the presence of Fe^{3+}. The higher Δ indicated the anisotropy in local environment of the probe atom due to the presence of Fe and Ti in close vicinity with the excess of 0.2 Li^+ ions occupying M_2 site. After the insertion of 0.5 Li^+ ions at the end plateau of 2.8 V, the presence of a new doublet with δ of 1.162 mm/s and Δ of 2.344 mm/s indicated the presence of Fe^{2+} after electrochemical reduction. Moreover, two reversible regions for Fe^{3+}/Fe^{2+} and Ti^{4+}/Ti^{3+} reactions during the

electrochemical lithium insertion were confirmed by Mössbauer technique. In the work performed by Novikova et al. [121], the electrochemical charge/discharge performance of $LiFe_{1-y}Mn_yPO_4/C$ nanocomposites was tested and the samples under gradual changes were characterized by Mössbauer spectroscopy. According to the parameters obtained from Mössbauer spectra, Mn was found distributed orderly so that each Fe ion only has one manganese ion in its nearest environment. In addition, the inhomogeneous distributions of Mn^{2+} and Mn^{3+} ions are formed in the interval when solid solutions exist in $Li_xFe_{0.7}Mn_{0.3}PO_4$.

Very recently, Asl et al. reported the synthesis of Li-containing iron borophosphate through a hydrothermal route [116]. Mössbauer spectroscopy was employed as an *ex-situ* technique to keep tracking of the oxidation state and environment change of iron as the cells were cycled between charged and discharged states at a rate of C/20. As shown in Fig. 7**A**, multiple doublet peaks with different Δ values and one doublet peak with the smaller Δ value were assigned to Fe^{2+} and Fe^{3+} in $Li_xFe(H_2O)_2[BP_2O_8]\cdot H_2O$, respectively. The Mössbauer spectrum of the sample charged to 4.0 V shows the percentage of Fe^{3+} about 68.8%. However, during the discharging process, the percentage of Fe^{3+} decreases to 47.7% and 34.0% as the cell potential decreases to 3.0 and 2.0 V, respectively. This trend demonstrates the fact that the mechanism of charge and discharge is associated with the oxidative deintercalation and reductive insertion, respectively.

4.2. Fe-based silicates

Polyoxyanion-type Fe-based silicates (Li_2FeSiO_4) with promising properties including nontoxicity and high theoretical capacity, have recently attracted a great deal of interest as cathode materials in new generations of LIBs [127,128]. In the work done by Chen et al. [112], the structural evolution of $Li_2Fe_{1-y}Mn_ySiO_4$ (y = 0, 0.2, 0.5, 1) powders during the first charge-discharge cycle was studied by applying Mössbauer spectroscopy. At fully discharged state, Mössbauer results show that the $LiFe^{3+}SiO_4$ and $Fe^{4+}SiO_4$ were reduced to Fe^{2+} and Fe^{3+} (majority). In contrast, at fully charged state, Fe^{2+} components were largely oxidized to Fe^{3+} in both $Li_2Fe_{0.8}Mn_{0.2}SiO_4$ and $Li_2Fe_{0.5}Mn_{0.5}SiO_4$. Because of the reduction of Mn^{3+} to Mn^{2+} is faster than that of Fe^{3+} to Fe^{2+}, only part of Fe^{3+} could be reduced to Fe^{2+} when the cell voltage reached 1.5 V. These results indicate that the capacity fading in the first few cycles could be ascribed to the instability of Mn^{3+} species, and the charge/discharge capacity in the subsequent cycles is dominated by the redox reaction of the Fe species. The *ex-situ* Mössbauer spectroscopy was also applied in a recent work from Chen et al. to probe the local disorder of Fe species at the octahedral FeO_6 sites and their valence states in the V-substituted and V-free samples [123]. The Fe^{3+}/Fe^{2+} and V^{4+}/V^{3+} redox couples were found contribute to the overall capacity performance and no evidence for the presence of Fe^{4+} species after charging to 4.8 V. Nevertheless, researches with the application of Mössbauer spectroscopy are still highly needed to provide further evidence of the electrochemical activity of the transition metals.

4.3. Fe-based polyanionic compounds

Massive Li-iron based polyanionic compounds have recently been applied for LIBs. Ahouari et al. confirmed the Li uptake-removal reversibility in $Fe_2(C_2O_4)_3\cdot 4H_2O$ by applying operando Mössbauer measurements [111], which were carried out during charge and discharge at C/10 rate (Fig. 7**B**). During discharging of the cell, the Mössbauer spectra show a narrow doublet that is assigned to Fe^{3+}, which progressively disappears while a new doublet with δ of 1.17 mm/s and Δ of 1.93 mm/s for typical Fe^{2+} appears and gradually becomes predominant. With subsequent charging up to 3.9 V, a reverse phenomenon with almost all Fe^{2+} oxidized to Fe^{3+} could be observed. The results demonstrate that the electrochemical activity occurred with a biphasic insertion process, linked to the Fe^{3+}/Fe^{2+} redox couple.

4.4. Sn-based nanomaterials

Sn-based nanomaterials have been recognized as high-energy density anode materials for rechargeable LIBs [129]. Mössbauer spectroscopy is also particularly powerful for elucidating the chemical environment of Sn, which technique has been widely used for getting insight into the reaction mechanism of Sn-based electrodes for LIBs [21,26,27,113,130]. For instance, Sathiya et al. applied the Mössbauer spectroscopy to investigate the redox activity and local structure of Sn in $Li_2Ru_{1-y}Sn_yO_3$ [27]. The variations of both the Δ and the spectrum absorption of the Mössbauer spectra indicate that the first charge triggers an irreversible distortion of the local structural around Sn. In addition, the Sn-O bonds were found weakened and strengthened with the extraction and insertion of Li, suggesting that Sn was less bounded to the oxygen network in charged samples. The results indicate that the cumulative anionic ($O^{2-} \rightarrow O_2^{2-}$) and cationic ($M^{n+} \rightarrow M^{(n+1)+}$) reversible redox processes are essential for the reactivity of these high-capacity materials towards Li. To investigate the electrochemical mechanism, Chamas et al. recently designed a modified Swagelok-type cell to carry out the in-situ Mössbauer measurements [113]. This method allows them to quantitatively follow the conversion reaction that transforms a nanostructured $FeSn_2$ based electrode into α-Fe/Li_7Sn_2 during the first discharge. By combining with the first principles calculations of the Mössbauer parameters, α-Fe/Li_7Sn_2 was considered as a real electrode material for cycling.

5. Applications of the Mössbauer technique in Fischer–Tropsch synthesis

5.1. Iron carbides

Fischer–Tropsch synthesis (FTS) has been considered as a crucial technology for the production of liquid fuel including unsustainable crude oil from carbon sources [131–133]. The wide availability, high adaptability to broad H_2/CO ratios and resistance to poisoning make Fe-based catalysts ideal for converting H_2-deficient syngas (CO and H_2) from renewable biomass or coal. Iron carbides are generally acknowledged as the main active phase in FTS, among which, Hagg carbide (χ-Fe_5C_2) and cementite (θ-Fe_3C) are mostly reported as heterogeneous catalysts for FTS. Iron carbides (ε'-$Fe_{2.2}C$, ε-Fe_2C) are sporadically identified active at comparative H_2/CO ratio and/or low temperature [134–136]. Mössbauer spectroscopy, as a unique technique that is powerful to identify all iron species, has been widely applied for identifying and quantifying the active phase of catalysts in FTS [28–35,40,125,137–144].

In the work done by Xu et al. [125], an ε-Fe_2C dominant catalyst was obtained when the carbonization of rapidly quenched skeletal iron (RQ Fe) occurred *in-situ* during LTFTS at 423–473 K. RQ Fe was found essential to overcome the seemingly insurmountable hindrance for directional carbidation of metallic iron to ε-Fe_2C. Mössbauer spectroscopy was applied to identify and quantify the phases of iron formed during FTS. As shown in Fig. 7**C**, the small sextet with a hyperfine magnetic field (*H*) of 329 kOe was assigned to metallic iron, while the other three sextets with *H* of 142, 172, and 235 kOe corroborated the formation of ε-Fe_2C. The intensity ratio of the three sextets is close to the theoretical value of 1: 4: 1.6, which corresponds to the ratio of individual crystallographic sites in ε-Fe_2C. The superparamagnetic (spm) doublet was assigned to Fe^{II} or Fe^{III} species, indicating the presence of poorly crystallized iron oxides. Therefore, ε-Fe_2C was identified as the main phase in the RQ Fe during LTFTS.

To further identify the active phases of the FTS catalysts, Mössbauer spectroscopy was monitored by Gnanamani et al. to identify and quantify the phase transformations of iron species during FTS [139]. As shown in Fig. 8, during FTS, iron oxide was converted to Fe_3O_4 (27%)

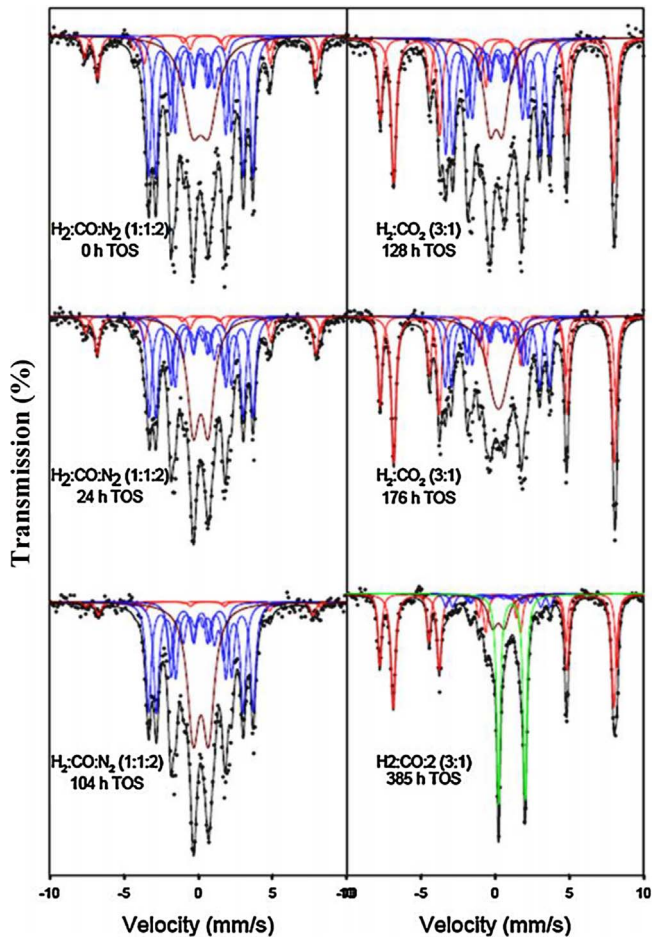

Fig. 8. Mössbauer spectra of α-Fe catalyst samples (20 K) obtained after activation and during FTS. The fitted curves are shown in solid lines: black, total spectra; red, oxide; blue, χ-Fe_5C_2; green, unknown FeO_x. (For interpretation of the references to colour in this figure legend, the reader is referred to the web version of this article.)
Source: Reproduced with permission from Ref. [139].

and χ-Fe_5C_2 (73%). Negligible change could be observed from the Mössbauer spectra of the samples obtained during the first 104 h of FTS, indicating little phase change during this period. However, the conversion of χ-Fe_5C_2 to Fe_3O_4 was found when switching from H_2: CO: N_2 (1:1:2) to H_2: CO_2 (3:1). The correlation between the rate of FTS and the percentage of Fe carbide suggests iron carbide as the main active phase for CO_2-based FTS.

Efforts were also made to investigate the effects of promoters and iron particle sizes on the stability of FTS catalysts. Recently, Xie et al. investigated the product selectivity, activity and stability of carbon nano fibers (CNF) supported Fe catalysts during Fischer-Tropsch to olefins (FTO) process [34]. The activity of unpromoted catalysts was found to increase over time, while the maximum activity of the catalysts with promoters was attained in the initial period and then deactivated prominently. *In-situ* Mössbauer spectroscopy was applied to clarify the relation between the phase and activity of the catalysts. Mössbauer results revealed that both promoted and unpromoted catalysts have a similar Fe carbidization level after reduction. However, after treatment in the synthesis gas for 20 h, the promoted catalyst was fully carbided while the unpromoted catalyst was carbided less than 25%. As the correlation between the percentage of Fe carbide species and the activity was not linear, the growth of the particle size was considered as the main reason for the deactivation of the FTS catalysts. In the recent work from Cho et al. [145], ZrO_2 as a structural promoter was incorporated into the Fe_2O_3 structures (denoted as FeZr(x), x represents the molar ratio of Zr/Fe). Mössbauer measurements carried out on the used FeZr(0), FerZr(0.3), and FeZr(1) reveal that the chemical compositions of the iron species were mainly in the forms of FeO, α-Fe_2O_3 and χ-Fe_5C_2. In addition the extent of χ-Fe_5C_2 formation was found to be much larger on the active FeZr(0.3), which also showed a higher activity and structural stability. The results indicate that the facile formation of χ-Fe_5C_2 is responsible for the higher C_{11}+ selectivity at a high CO conversion.

Through a combination of *in-situ* DRIFTS, XAFS and Mössbauer study, Wezendonk et al. investigated the changes in electronic, structural, and local environments of Fe during pyrolysis of Fe-BTC as highly active and stable FTS catalysts (Fe@C) [35]. Mössbauer results revealed the formation of highly dispersed ε'-$Fe_{2.2}C$ when pyrolysis of Fe-BTC at 400 °C, while χ-Fe_5C_2 became the main phase when pyrolysis at 600 °C. Due to the extensive sintering and carburization above these temperatures, θ-Fe_3C appeared as the predominant phase when pyrolysis was done at 900 °C. Therefore, by changing the pyrolysis temperature of Fe-BTC, both the particle size and phase of the Fe@C could be modulated, which was considered as a promising way to obtain highly active and stable FTS catalysts. Recently, *in-situ* Mössbauer spectroscopy was applied by Santos et al. to unravel the role of the Fe-Ti interactions on the high temperature FTS (HRFTS) catalyst performance and stability [146]. The *in-situ* Mössbauer results reveal that the reduction degree of iron species decreases significantly with the Ti/Fe ratio. For example, the reduced $Fe_{2.1}Ti$ is composed of 74% Fe^0, 5% Fe_2TiO_5 and 21% Fe^{II}, while the reduced $Fe_{8.7}Ti$ is mostly composed of Fe^0. Therefore, an appropriate amount of pseudrobrookite (<13 wt.%) could enhance the carburization degree and minimized the re-oxidation of carbides during syngas conversion, thus improving the HRFTS performance.

6. Applications of the Mössbauer technique in biomass conversion

Biomass is one of the most important renewable carbon resources, and it is regarded as the ideal feedstock to replace petroleum for the production of chemicals and fuels [147]. Over the past decades, great efforts have been dedicated to biomass conversion due to the fossil fuel depletion and environmental problems. Some new reaction pathways have been developed and some novel catalysts have been designed [148,149]. Additionally, some sensitive characterization technologies have also been used in biomass conversion, and helped to disclose the "black box" of catalytic reaction [150]. Mössbauer spectroscopy possesses the highest resolution among all of the spectroscopic techniques, which is sensitive to some special catalysts [151]. Recently, iron and tin Mössbauer spectroscopy were used to unveil the structure of catalysts for biomass conversion such as the tin-zeolite catalysts for sugar conversion to lactic acid and sugar isomerization, tin based bimetallic catalysts for cellulose hydrocracking, iron based catalysts for biomass gasification, lignin fragmentation and hydrodeoxygenation reactions. Herein, we cannot cover all reactions that are involved in using Mössbauer spectroscopy, but mainly focus on some typical examples that use Mössbauer spectroscopy to understand the reaction and catalysts in biomass conversion.

6.1. Tin-Beta catalysts

Tin-Beta catalysts were first synthesized by Corma et al. for Baeyer-Villiger oxidations [152]. In 2010, Holm et al. first applied it in the conversion of sugars to lactic acid derivatives. The Lewis acidic zeotypes of Sn-Beta are very active for mono- and disaccharides conversion, which produced 68% yield of methyl lactate in methanol at 160 °C for 20 h with sucrose as the substrate [153]. Afterwards, great efforts were conducted on developing new catalysts to elevate the yield of products. However, the structure of tin in catalysts and the distribution of active sites are not fully determined. Wolf et al. employed Mössbauer spectroscopy combined with NMR to examine the structural information of the active-site speciation in Sn-Beta zeolite. They performed the ^{119}Sn Mössbauer spectroscopy at different temperatures, and found that

all spectra show a doublet with Δ of 0.75 mm/s and δ of 0.07 mm/s, indicating a hexacoordinated Sn^{IV} site with a distorted geometry. Based on the increase of the relative spectral area between 300 K and 15 K and some other characterizations, they concluded that Sn signals should be assigned to the framework of zeolite, and the active sites of Sn-Beta zeolite should be corresponding to octahedrally coordinated Sn^{IV} involving the tetrahedral Sn-sites with two water molecules [154]. Dijkmans et al. performed the Mössbauer spectroscopy of Sn/DeAlBeta catalysts after treatment at 1023 K in H_2. Two types of tin sites were observed, one has an δ of −0.24 mm/s and a Δ of 0.50 mm/s that should be attributed to the tetrahedral Sn^{IV} species, and the other one has an δ of 3.05 mm/s and a Δ of 2.08 mm/s that corresponds to the shift and splitting profile characteristic of Sn^{II} species accounting for 81% of tin in zeolites. Significantly higher temperatures are required for reduction of the single site Sn-atoms in Sn-Beta as compared to nanosized SnO_2 due to the strong interaction of Sn^{IV} with the zeolite support. Finally, they proposed the structure of Lewis acid sites in tin-zeolite under different conditions [155].

6.2. Multi-metallic catalysts

Mössbauer spectroscopy is also applied in characterizing bimetallic catalysts in biomass conversion, especially, in conversion of biomass to glycols. Xiao et al. prepared Cu–Fe catalysts by an epoxide-assisted process for glycerol hydrogenolysis. The highest glycerol conversion of 47% was obtained at 92% 1,2-propylene glycol (1,2-PG) selectivity over the CuFe-500 catalyst under the conditions of 190 °C, 4.1 MPa initial H_2 pressure for 10 h. According to the Mössbauer spectroscopy results, one can find a crystalline phase transformation from cubic to tetragonal $CuFe_2O_4$ with elevating calcination temperature, and the formation of spinel $CuFe_2O_4$ over the CuFe-500 catalyst could greatly enhance the activity for glycerol conversion [156]. Cellulose is the most abundant non-edible feedstock for biomass conversion, and it is very attractive to convert it into glycols. In 2008, Ji et al. first explored the one-pot conversion of cellulose to glycols, i.e., ethylene glycol (EG) and 1,2-PG, over tungsten based catalysts [157]. Since then, this reaction has gained great attention because of the versatile application of glycols and abundant renewable feedstock [158,159]. Recently, Sun et al. extended catalysts to bimetallic catalysts, and used Sn species with different valences in combination with Ni catalysts for cellulose conversion. They found that under hydrogenation catalysts conditions, the metallic Sn showed high activity toward EG (57.6%) in contrast to SnO that favored the formation of 1,2-PG (32.2%). The reason for the high activity of composite catalysts was investigated by Mössbauer spectroscopy and other technologies. The results demonstrated that 85.6% of tin sites with an δ of 1.8 mm/s should be attributed to the NiSn alloy in the Ni−Sn(90)/AC catalyst, only 14.4% tin sites with an δ of about −0.02 mm/s was attributed to the Sn (IV). Therefore, the Sn species in NiSn alloy in-situ formed from metallic Ni and Sn powders are the active sites for the high selectivity of glycols, which was confirmed by TEM and conditional experiments [160].

Lignin is an irregular phenolic copolymer with a three dimensional methoxylated phenylpropane structures in biomass. Catalytic conversion of lignin over heterogeneous catalysts still poses a great challenge due to its inert structure. Olcese et al. investigated the catalytic hydrodeoxygenation of guaiacol over Fe/SiO_2 catalysts as a model reaction of lignin pyrolysis in a fixed-bed reactor. A sextet characteristic and several small contributions were observed, which were estimated to about 85%, 3% and 12% for Fe, Fe_3O_4 and the carbide phase, respectively, and the majority phase of iron should be the active sites for guaiacol conversion [161]. Opris et al. synthesized $Co@Nb_2O_5@Fe_3O_4$ catalysts for lignin fragmentation; the catalysts and unreacted lignin could be separated easily over the magnetic composite without affecting the reaction activity of metal catalysts. The authors confirmed the presence of magnetic nanoparticles with 20 nm particle size by Mössbauer patterns at different temperatures [162].

Besides used in sugar and lignin conversion, Mössbauer spectroscopy is also a powerful tool to investigate the catalysts used in biomass gasification or model compounds conversion. Virginie et al. used the Fe/olivine catalyst synthesized using an optimized impregnation method for biomass gasification in a dual fluidized bed. Fe/olivine material acts as a catalyst for hydrocarbon and tar reforming. In addition, it may act as an oxygen carrier, which could transfer oxygen from the combustor to the gasifier, and part of the oxygen could be also used to burn volatile compounds. The composition of olivine and catalysts were characterized by Mössbauer spectroscopy and XRD under different conditions. Two doublets and three sextets were present, which were attributed to the Fe^{2+} of wustite FeO and Fe^{3+}, Fe^{2+} in tetrahedral sites and octahedral sites of the spinel Fe_3O_4. The authors quantified different ion species in catalysts and found that catalyst structure could be maintained despite the large number of redox cycles during the reactions [163]. Yang et al. modified the Pd/SiO_2 catalysts by FeO_x species for the solvent-free hydrodeoxygenation of the aldol condensation product of furfural and methyl-isobutylketone to fuels. According to the *quasi-in-situ* Mössbauer spectra of typical catalysts, they found that the modification of Pd/SiO_2 with iron species led to the generation of Pd-Fe alloy and partially reduced FeOx species, which restrained the decarbonylation reaction and retro-aldol condensation by promoting the hydrogenation of carbonyl groups [164]. Chen et al. employed Fe-substituted Ni−Si intermetallic catalysts for removal of dibenzothiophene by hydrodesulfurization. The $Ni_{1-x}Fe_xSi_2$ catalysts significantly improved the hydrogenation activity.

The Mössbauer spectra of Fe-substituted Ni−Si intermetallics are shown in Fig. 9, the doublet with δ = 0.27 mm/s and Δ = 0.43 mm/s was assigned to FeSi, while the sextet was attributed to $FeNi_3$. The singlet with the δ = − 0.03 mm/s could be ascribed to cubic silicide like $FeSi_2$. The results reveal that Fe atoms preferentially bonded with Ni to form alloy and combined with Si to form silicide, which led to a strong modification of geometry and electronic structure of the metals, and resulted in a high activity for the hydrodesulfurization of dibenzothiophene [165].

As we discussed above, Mössbauer spectroscopy has been used in many aspects of catalyst characterizations involving in biomass conversion. However, it is still a challenge to disclose the structure of catalysts solely by Mössbauer spectroscopy, many other novel technologies should be used to confirm the results. Moreover, more *in-situ* Mössbauer spectroscopy or reactions should be developed for studying the states of catalysts under reaction conditions.

7. Applications of the Mössbauer technique in N_2O decomposition

The decomposition of N_2O has received much attention in recent years, which provides a solution to mitigate nitrous oxide that is formed as a byproduct of ammonia oxidation over the Pt-Rh alloy gauzes in the nitric acid plants [166]. Various catalysts have been reported to show activity for the N_2O abatement, such as zeolites [167–169], perovskites [170] and ex-hydrotalcites [171]. On the other hand, N_2O as propellant is used in small satellite propulsion systems. The concentration of propellant N_2O must be high enough to generate large propulsion power during its decomposition. Thus, quite a large amount of heat is released, which challenges the stability of catalysts at very high temperatures. Metal-substituted hexaaluminates are considered as promising catalysts for the decomposition of N_2O as propellant thanks to its peculiar layered structure consisting of γ-Al_2O_3 spinel blocks intercalated by mirror planes where large cations (Ba or La) are located [172]. In the following section, some advances on unveiling the nature of active species in Fe/zeolite, and hexaaluminate catalysts for the decomposition of N_2O using ^{57}Fe Mössbauer spectroscopy were covered.

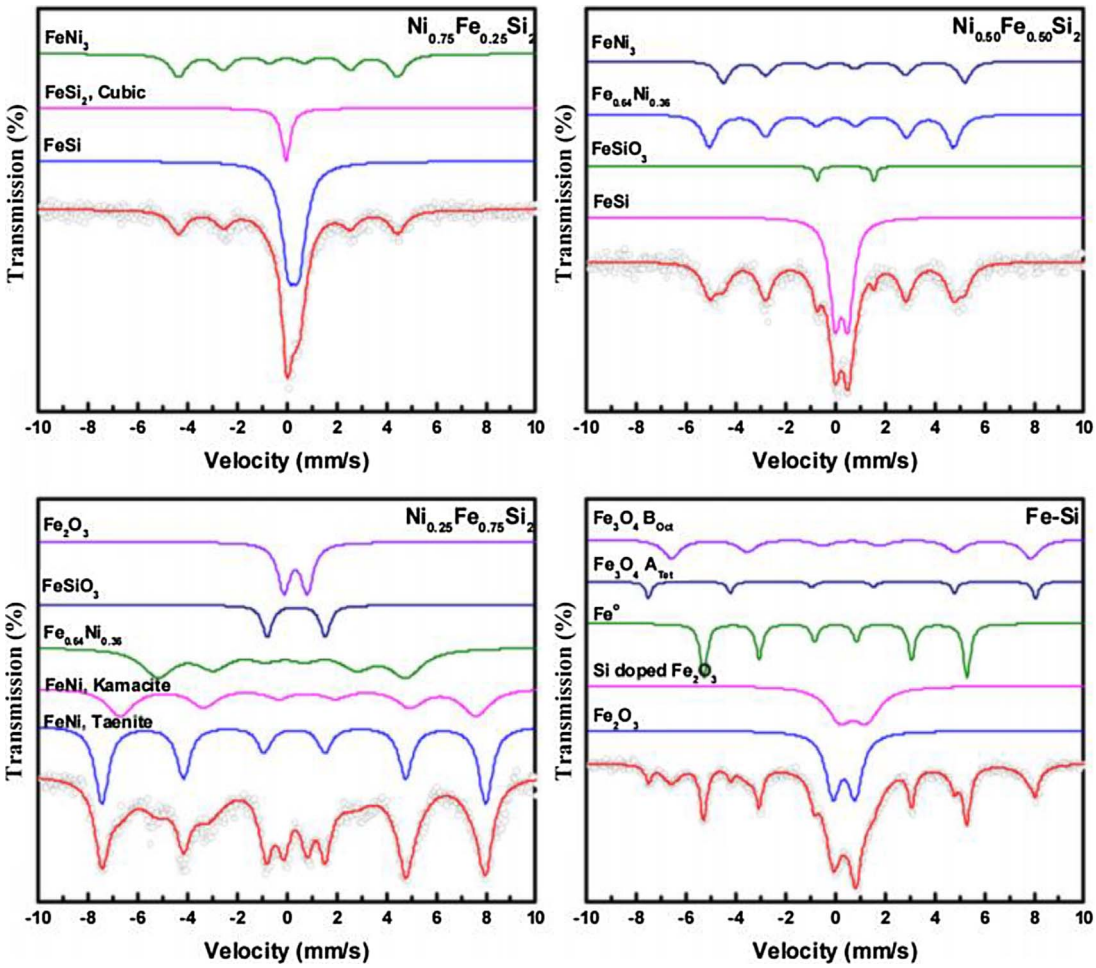

Fig. 9. ^{57}Fe Mössbauer spectra of Fe-substituted Ni – Si intermetallics.
Source: Reproduced with permission from Ref. [165].

7.1. Fe/zeolites

Fe/zeolite is a class of popular catalysts reported for the decomposition of N_2O. The influence of preparation methods, topology of zeolites and Fe content as well as reaction mechanism and kinetics have been investigated in details [42,173,174]. However, the nature of active Fe species is still controversial. Sazama et al. [44] elucidated Fe species including Fe ions, Fe-oxo oligomers and Fe-oxo species in non-steamed (FeH-ZSM-5) and steamed Fe-ZSM-5 (Fe(H)-ZSM-5st) using semi-quantitative Mössbauer spectroscopy combined with FTIR, UV–vis and H_2-TPR. It was found that the evacuated non-steamed FeH-ZSM-5 contained mainly bare Fe^{II} ions (72%), oligomeric Fe^{III}-oxo species (9–12%) and dinuclear Fe^{III} (16–19%) while the steamed Fe(H)-ZSM–5 st were largely reorganized, leading to the significant decrease in the concentration of bare Fe^{II} ions (15–16%) and the appearance of T_d-coordinated Fe^{III} ions in the Fe-Al-Si extra-framework species (43–47%) and Fe-oxide-like particles (30–33%). Mössbauer spectroscopy of these two samples after interaction with N_2O at 400 °C presented that bare Fe^{II} ions were partially and completely converted to form a new Fe species attributed to Fe^{III}-O^-, indicating that bare Fe^{II} ions were highly active for N_2O decomposition. Fe(H)-ZSM–5st had more bare Fe^{II} ions than FeH-ZSM-5, thereby higher activity for N_2O decomposition were obtained for this catalyst. Mössbauer spectroscopy was applied to study the effect of the distribution of Al atoms in the structure on the state of incorporated Fe species in Fe/HZSM-5 catalysts. The authors found that Al pairs in the framework could greatly stabilize the most active sites of bare Fe^{II} ions and $[Fe^{II}–O–Fe^{II}]^{2+}$ complexes even in oxidizing atmosphere [175]. Moretti et al. found that the nature of Fe species was highly dependent on the amount of Fe loaded in Fe/S-1 catalysts [43]. In $[Fe_{1.4}]$-S-1 sample with Fe loadings of 1.31 wt%, more than half of total Fe ions were attributed to high-spin Fe^{3+} ions in tetrahedral framework coordination and the remaining absorption was assigned to high-spin extra-framework iron ions in octahedral coordination. In $[Fe_{1.6}]$-S-1 sample with Fe loadings of 1.48 wt %, only extra-framework Fe_xO_y nanoparticles were observed with the particle size larger (< 20 nm) than those in $[Fe_{1.4}]$-S-1 sample (< 1 nm). Activity test results showed that the overgrowth of Fe-oxide like species is essential for the decomposition of N_2O.

Boroń et al. reported BEA zeolite modified with iron catalysts for N_2O decomposition [176]. The Mössbauer spectrum of Fe1.0SiBEA shows two dominant doublets ($0.18 \leq \delta \leq 0.23$ mm/s), which are characteristic of iron Fe^{3+} species in pseudo-tetrahedral surroundings, and the small singlet is characteristic of the Fe^{4+} species (Fig. 10). The results indicate that the Fe^{3+} incorporated into pseudo-tetrahedral framework of SiBEA zeolite at low Fe content (< 2 wt%). At higher Fe contents, extra-framework octahedral Fe^{3+} species were also identified. The highest catalytic activity for N_2O decomposition was obtained from the $Fe_{4.0}$AlSiBEA sample which contained iron mainly as the framework pseudo-tetrahedral Fe^{3+}. Wang et al. studied the influence of extra-framework Al in Fe/ZSM-35 and observed the generation of a bi-nuclear Fe sites stabilized by extra-framework Al species [177]. Activity test results presented that extra-framework Al species could promote the formation of active Fe sites for N_2O decomposition. Xie et al. compared the activity of Fe_2O_3/Silicalite-1, Fe-Silicalite-1, Fe_2O_3/Fe-Silicalite-1 for N_2O decomposition and found that Fe_2O_3/Fe-Silicalite-1 nanowires showed the highest activity [178]. Mössbauer spectra of

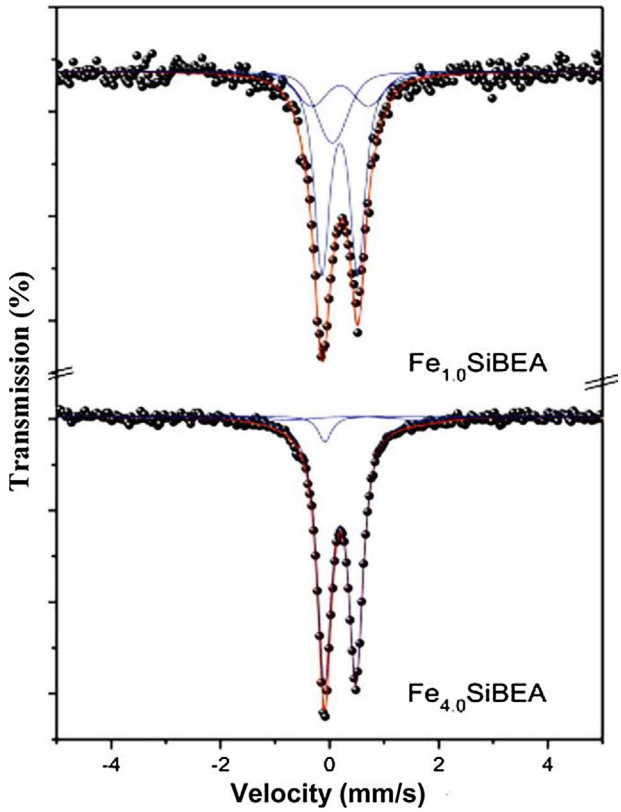

Fig. 10. Room temperature ^{57}Fe Mössbauer spectra of $Fe_{4.0}$SiBEA and $Fe_{1.0}$SiBEA. *Source*: Reproduced with permission from Ref. [176].

Fe_2O_3/Fe-Silicalite-1 nanowires were fitted with two doublets, attributed to iron ions in the silicalite-1 framework and small Fe_2O_3 nanoparticles, respectively. In comparison, a sextet with magnetic splitting associated with large Fe_2O_3 particles was observed for Fe_2O_3/Silicalite-1. Combined with activity test, it could be concluded that small Fe_2O_3 nanoparticles with size of 1–2 nm were the main active sites for N_2O decomposition.

7.2. Hexaaluminates

In 2007, our group for the first time reported the novel $BaIr_yFe_{1-y}Al_{11}O_{19}$ (y = 0.2, 0.5 and 0.8) (BIFA) catalysts showing not only high activity but also excellent stability for the decomposition of N_2O as propellant [179,180]. Nevertheless, the chemical state of Ir ions and their relationship with the catalytic activity was unclear due to the difficulty in characterization. We employed H_2-reduction ^{57}Fe Mössbauer spectroscopy combined with Rietveld refinement to indentify the crystallographic site of Ir indirectly, which provides the direction of designing the noble metals-substituted hexaaluminates with high activity for N_2O decomposition [181,182]. Recently, we attempted to stabilize the Ru ions, regarded to be active for N_2O decomposition [183]. ^{57}Fe Mössbauer spectroscopy after H_2 reduction at 350 °C for 2 h presented that only Fe^{3+} ions occupied the tetrahedral Al(2) sites in the spinel block, and the Ru ions in the tetrahedral Al(5) sites accounted for the high activity for N_2O decomposition.

The good catalytic performance of the metal-substituted hexaaluminates originates from the active metal ions which could be stabilized in their lattice. However, the stabilization mechanism of the metal ions is still unclear due to the lack of effective characterization techniques. By applying Mössbauer spectroscopy combined with Rietveld refinement, our group used Fe as a probe to investigate the local environments of the substituted transition metal ions in hexaaluminate and proposed a mechanism of stabilization of Fe ions in Ba-hexaaluminate at the molecular level [138,184] and this work has been reviewed by Liu et al. [2]. Compared to Ba-hexaaluminates, La-hexaaluminates with the MP structure possess more Al sites in the mirror plane, which are generally considered to be associated with catalytic activity. Therefore, by applying Mössbauer spectroscopy, we further investigated the Fe-substituted La-hexaaluminates concentrating on the evolution of the chemical state of Fe ions during calcination [185,186]. Fe^{3+} ions from the initial α-Fe_2O_3 mainly occupy the tetrahedral Al(2) and Al(5) sites while those from the $LaFeO_3$ intermediates preferentially enter into the octahedral Al(3) sites in the mirror plane of La-hexaaluminates. These results indicate that Fe^{3+} ions in the Al(3) and Al(5) sites are responsible for N_2O decomposition by correlating the normalized rates of the catalysts at 500 °C.

8. Summary and concluding remarks

Mössbauer spectroscopy offers a powerful tool to characterize the local electronic structure of the probe-element in nano-structured or amorphous materials, crystalline and glass by determining the local coordination, bonding and oxidation state. It is beneficial for the identification of the redox processes and characterization of intermediate phases, making the study of catalytic mechanism become possible. Recent years have witnessed a blossoming interest in applying Mössbauer technique in various catalysis fields such as photocatalysis, Fenton-like reaction, electrocatalysis, LIBs, FTS, biomass conversion, N_2O decomposition and etc. For each application field, we illustrated how this technique has helped to identify the main active sites among various Fe/Sn-based catalysts systems and how that knowledge has led to successful strategies to investigate the reaction mechanism. The knowledge of probing the local electronic structure, investigating the redox cycling, identifying the active site, determining the crystal phase, and tracking the oxidation state and environment change of various Fe-based catalysts with the application of Mössbauer technique are of great importance for the further development in these catalysis fields.

Nevertheless, the future research in these fields will rely on the advances in analytical instrumentation. For instance, the impact of Fe doping on the electronic structure of TiO_2 as well as the redox cycles and active sites of Fenton-like catalysts could be further identified with the combination of other advanced methods such as X-ray spectrometry, which will enormously increase the potential of Mössbauer spectroscopy as an analytical tool and benefit the identification of the oxidation state and environment change of Fe in Fe-based silicates, phosphates and polyanionic compounds between charge and discharge states of LIBs. The active site of Fe-N-C and NiFe based materials as electrocatalysts could be clearly probed with the development of *in-situ* or quasi *in-situ* reactors to operando analysis the properties of catalysts. Further development of high temperature *in-situ* or quasi *in-situ* reactors would greatly promote the investigation of the phase transformation of iron carbides as catalysts during or after FTS. In addition, compared with conventional Mössbauer spectroscopy, nuclear forward scattering (NFS) allows studying hyperfine interactions with much smaller samples and much shorter measuring times, Nuclear inelastic scattering (NIS) allows investigating local phonon spectra at the Mössbauer probe nucleus, both of them are certainly on their way to a great future.

Acknowledgements

This work was supported by the National Natural Science Foundation of China (11079036, 21476232) and the Chinese Academy of Sciences Visiting Professorships for Senior International Scientists (2011T1G15) as well as the Chinese Academy of Sciences for “100 Talents” Project. This work was also partially supported by the China Ministry of Science and Technology under the Contract of 2016YFA0202804. Many thanks to the anonymous reviewers who have helped improve this paper.

References

[1] P. Gutlich, Z. Anorg, Allg. Chem. 638 (2012) 15–43.
[2] K. Liu, A.I. Rykov, J.H. Wang, T. Zhang, F.C. Jentoft (Ed.), Adv. Catal. 58 (2015) 1–142.
[3] C. Andriamiadamanana, C. Laberty-Robert, M.T. Sougrati, S. Casale, C. Davoisne, S. Patra, F. Sauvage, Inorg. Chem. 53 (2014) 10129–10139.
[4] T. Kawauchi, N. Nagatsuka, K. Fukutani, Hyperfine Interact. (2016) 73–80.
[5] L.V.C. Lima, M. Rodriguez, V.A.A. Freitas, T.E. Souza, A.E.H. Machado, A.O.T. Patrocinio, J.D. Fabris, L.C.A. Oliveira, M.C. Pereira, Appl. Catal. B 165 (2015) 579–588.
[6] T.C. Araujo, H.D. Oliveira, J.J.S. Teles, J.D. Fabris, L.C.A. Oliveira, J.P. de Mesquita, Appl. Catal. B 182 (2016) 204–212.
[7] W.Q. Li, A. Kuc, C.F.J. Walther, T. Heine, J. Phys. Chem. A 119 (2015) 5742–5748.
[8] E. Courtin, G. Baldinozzi, M.T. Sougrati, L. Stievano, C. Sanchez, C. Laberty-Robert, J. Mater. Chem. A 2 (2014) 6567–6577.
[9] I.S.X. Pinto, P. Pacheco, J.V. Coelho, E. Lorencon, J.D. Ardisson, J.D. Fabris, P.P. de Souza, K.W.H. Krambrock, L.C.A. Oliveira, M.C. Pereira, Appl. Catal. B 119 (2012) 175–182.
[10] G. Satishkumar, M.V. Landau, T. Buzaglo, L. Frimet, M. Ferentz, R. Vidruk, F. Wagner, Y. Gal, M. Herskowitz, Appl. Catal. B 138 (2013) 276–284.
[11] J.V. Coelho, M.S. Guedes, R.G. Prado, J. Tronto, J.D. Ardisson, M.C. Pereira, L.C.A. Oliveira, Appl. Catal. B 144 (2014) 792–799.
[12] Q. Sun, M. Liu, K.Y. Li, Y. Zuo, Y.T. Han, J.H. Wang, C.S. Song, G.L. Zhang, X.W. Guo, CrystEngComm 17 (2015) 7160–7168.
[13] F.F. Dias, A.A.S. Oliveira, A.P. Arcanjo, F.C.C. Moura, J.G.A. Pacheco, Appl. Catal. B 186 (2016) 136–142.
[14] A.M. Mesquita, I.R. Guimaraes, G.M.M. de Castro, M.A. Goncalves, T.C. Ramalho, M.C. Guerreiro, Appl. Catal. B 192 (2016) 286–295.
[15] U.I. Kramm, M. Lefevre, N. Larouche, D. Schmeisser, J.P. Dodelet, J. Am. Chem. Soc. 136 (2014) 978–985.
[16] J.A. Varnell, E.C.M. Tse, C.E. Schulz, T.T. Fister, R.T. Haasch, J. Timoshenko, A.I. Frenkel, A.A. Gewirth, Nat. Commun. 7 (2016) 12582–12590.
[17] M. Lefevre, E. Proietti, F. Jaouen, J.P. Dodelet, Science 324 (2009) 71–74.
[18] Q. Jia, N. Ramaswamy, H. Hafiz, U. Tylus, K. Strickland, G. Wu, B. Barbiellini, A. Bansil, E.F. Holby, P. Zelenay, S. Mukerjee, ACS Nano 9 (2015) 12496–12505.
[19] A. Serov, K. Artyushkova, E. Niangar, C.M. Wang, N. Dale, F. Jaouen, M.T. Sougrati, Q.Y. Jia, S. Mukerjee, P. Atanassov, Nano Energy 16 (2015) 293–300.
[20] N.R. Sahraie, U.I. Kramm, J. Steinberg, Y.J. Zhang, A. Thomas, T. Reier, J.P. Paraknowitsch, P. Strasser, Nat. Commun. 6 (2015) 8618–8626.
[21] L. Baggetto, H.-Y. Hah, J.-C. Jumas, C.E. Johnson, J.A. Johnson, J.K. Keum, C.A. Bridges, G.M. Veith, J. Power Sources 267 (2014) 329–336.
[22] S.R. Bruno, C.K. Blakely, J.B. Clapham, J.D. Davis, W. Bi, E.E. Alp, V.V. Poltavets, J. Power Sources 273 (2015) 396–403.
[23] A.S. Christiansen, R.E. Johnsen, P. Norby, C. Frandsen, S. Morup, S.H. Jensen, K.K. Hansen, P. Holtappels, J. Electrochem. Soc. 162 (2015) A531–A537.
[24] E. McCalla, A. Abakumov, G. Rousse, M. Reynaud, M.T. Sougrati, B. Budic, A. Mahmoud, R. Dominko, G. Van Tendeloo, R.P. Hermann, J.-M. Tarascon, Chem. Mater. 27 (2015) 1699–1708.
[25] M. Biswal, A. Suryawanshi, V. Thakare, S. Jouen, B. Hannoyer, V. Aravindan, S. Madhavi, S. Ogale, J. Mater. Chem. A 1 (2013) 13932–13940.
[26] L. Protesescu, A.J. Rossini, D. Kriegner, M. Valla, A. de Kergommeaux, M. Walter, K.V. Kravchyk, M. Nachtegaal, J. Stangl, B. Malaman, P. Reiss, A. Lesage, L. Emsley, C. Coperet, M.V. Kovalenko, Acs Nano 8 (2014) 2639–2648.
[27] M. Sathiya, G. Rousse, K. Ramesha, C.P. Laisa, H. Vezin, M.T. Sougrati, M.L. Doublet, D. Foix, D. Gonbeau, W. Walker, A.S. Prakash, M. Ben Hassine, L. Dupont, J.M. Tarascon, Nature Mater. 12 (2013) 827–835.
[28] H.Y. Suo, S.G. Wang, C.H. Zhang, J. Xu, B.S. Wu, Y. Yang, H.W. Xiang, Y.W. Li, J. Catal. 286 (2012) 111–123.
[29] H.J. Schulte, B. Graf, W. Xia, M. Muhler, Chemcatchem 4 (2012) 350–355.
[30] Z.Q. Yang, X.L. Pan, J.H. Wang, X.H. Bao, Catal. Today 186 (2012) 121–127.
[31] X.-W. Liu, S. Zhao, Y. Meng, Q. Peng, A.K. Dearden, C.-F. Huo, Y. Yang, Y.-W. Li, X.-D. Wen, Sci. Rep. 6 (2016) 26184–26193.
[32] W. Ma, G. Jacobs, G.A. Thomas, W.D. Shafer, D.E. Sparks, H.H. Hamdeh, B.H. Davis, ACS Catal. 5 (2015) 3124–3136.
[33] Y. Liu, J.-F. Chen, J. Bao, Y. Zhang, ACS Catal. 5 (2015) 3905–3909.
[34] J. Xie, H.M.T. Galvis, A.C.J. Koeken, A. Kirilin, A.I. Dugulan, M. Ruitenbeek, K.P. de Jong, ACS Catal. 6 (2016) 4017–4024.
[35] T.A. Wezendonk, V.P. Santos, M.A. Nasalevich, Q.S.E. Warringa, A.I. Dugulan, A. Chojecki, A.C.J. Koeken, M. Ruitenbeek, G. Meima, H.-U. Islam, G. Sankar, M. Makkee, F. Kapteijn, J. Gascon, ACS Catal. 6 (2016) 3236–3247.
[36] M. Virginie, J. Adanez, C. Courson, L.F. de Diego, F. Garcia-Labiano, D. Niznansky, A. Kiennemann, P. Gayan, A. Abad, Appl. Catal. B 121 (2012) 214–222.
[37] R.Y. Sun, M.Y. Zheng, J.F. Pang, X. Liu, J.H. Wang, X.L. Pan, A.Q. Wang, X.D. Wang, T. Zhang, ACS Catal. 6 (2016) 191–201.
[38] W.P. Ma, G. Jacob, D.E. Sparks, W.D. Shafer, H.H. Hamdeh, S.D. Hopps, V.R.R. Pendyala, Y.F. Hu, Q.F. Xiao, B.H. Davis, Appl. Catal. A- Gen. 513 (2016) 127–137.
[39] F.G. Mendonca, J.P.M. Gomes, J.C. Tristao, J.D. Ardisson, R.R. Soares, R.M. Lago, Fuel 184 (2016) 36–41.
[40] Q.G. Yan, C.X. Wan, J. Liu, J.S. Gao, F. Yu, J.L. Zhang, Z.Y. Cai, Green Chem. 15 (2013) 1631–1640.
[41] J.X. Xie, H.M.T. Galvis, A.C.J. Koeken, A. Kirilin, A.I. Dugulan, M. Ruitenbeek, K.P. de Jong, ACS Catal. 6 (2016) 4017–4024.
[42] J.Y. Wang, G.N. Li, X.H. Ju, H.A. Xia, F.T. Fan, J.H. Wang, Z.C. Feng, C. Li, J. Catal. 301 (2013) 77–82.
[43] G. Moretti, G. Fierro, G. Ferraris, G.B. Andreozzi, V. Naticchioni, J. Catal. 318 (2014) 1–13.
[44] P. Sazama, B. Wichterlova, E. Tabor, P. Stastny, N.K. Sathu, Z. Sobalik, J. Dedecek, S. Sklenak, P. Klein, A. Vondrova, J. Catal. 312 (2014) 123–138.
[45] W.G. Li, G. Li, C.Z. Jin, X. Liu, J.H. Wang, J. Mater. Chem. A 3 (2015) 14786–14793.
[46] F. Huang, X.D. Wang, A.Q. Wang, J.M. Xu, T. Zhang, Catal. Sci. Technol. 6 (2016) 4962–4969.
[47] M. Jablonska, G. Delahay, K. Kruczala, A. Blachowski, K.A. Tarach, K. Brylewska, C. Petitto, K. Gora-Marek, J. Phys. Chem. C 120 (2016) 16831–16842.
[48] I. Kocemba, J. Rynkowski, J. Gurgul, R.P. Socha, K. Latka, J.M. Krafft, S. Dzwigaj, Appl. Catal. A- Gen. 519 (2016) 16–26.
[49] J.M.M. Millet, in: B.C. Gates, H. Knozinger (Eds.), Advances in Catalysis, 51, 2007, 309–350.
[50] L. Liu, Y. Jiang, H. Zhao, J. Chen, J. Cheng, K. Yang, Y. Li, ACS Catal. 6 (2016) 1097–1108.
[51] M. Wang, D. Wang, Z. Li, Appl. Catal. B 183 (2016) 47–52.
[52] Y. Yan, Y. Yu, D. Wu, Y. Yang, Y. Cao, Nanoscale 8 (2016) 949–958.
[53] J. Soria, J.C. Conesa, V. Augugliaro, L. Palmisano, M. Schiavello, A. Sclafani, J. Phys. Chem. 95 (1991) 274–282.
[54] S. Kment, F. Riboni, S. Pausova, L. Wang, L. Wang, H. Han, Z. Hubicka, J. Krysa, P. Schmuki, R. Zboril, Chem. Soc. Rev. 46 (2017) 3716–3769.
[55] É.G. Bajnóczi, N. Balázs, K. Mogyorósi, D.F. Srankó, Z. Pap, Z. Ambrus, S.E. Canton, K. Norén, E. Kuzmann, A. Vértes, Z. Homonnay, A. Oszkó, I. Pálinkó, P. Sipos, Appl. Catal. B 103 (2011) 232–239.
[56] T. Tsoncheva, R. Ivanova, J. Henych, N. Velinov, M. Kormunda, M. Dimitrov, D. Paneva, M. Slusna, I. Mitov, V. Stengl, Catal. Commun. 81 (2016) 14–19.
[57] A. Magdziarz, J.C. Colmenares, O. Chernyayeva, D. Lisovytskiy, J. Grzonka, K. Kurzydlowski, K. Freindl, J. Korecki, Ultrason. Sonochem. 38 (2017) 189–196.
[58] F.H. Yu, Y.J. Wang, H.L. Tang, Y.J. Zhang, C.Z. Jin, X. Liu, M.R. Li, J.H. Wang, Catal. Commun. 51 (2014) 46–52.
[59] Y.J. Wang, Y.J. Zhang, F.H. Yu, C.Z. Jin, X. Liu, J.Y. Ma, Y. Wang, Y.Y. Huang, J.H. Wang, Catal. Today 258 (2015) 112–119.
[60] K. Sivula, F. Le Formal, M. Gratzel, Chem. Mater. 21 (2009) 2862–2867.
[61] Y. Wang, T. Yu, X.Y. Chen, H.T. Zhang, S.X. Ouyang, Z.S. Li, J.H. Ye, Z.G. Zou, J. Phys. D Appl. Phys. 40 (2007) 3925–3930.
[62] W.J. Luo, T. Yu, Y.M. Wang, Z.S. Li, J.H. Ye, Z.G. Zou, J. Phys. D Appl. Phys. 40 (2007) 1091–1096.
[63] V.A.A. Freitas, L.A. Maia, R.E. Belardinelli, J.D. Ardisson, M.C. Pereira, L.C.A. Oliveira, Environ. Sci. Pollut. Res. Int. 24 (2017) 6114–6125.
[64] A.C. da Silva, C.G.O. Bruziquesi, M.R. Almeida, M. Rodriguez, H.S. Oliveira, A.R.T. Machado, L.C.A. Oliveira, M.C. Pereira, J. Photoch. Photo. A 335 (2017) 259–267.
[65] H.S. Oliveira, L.C.A. Oliveira, M.C. Pereira, J.D. Ardisson, P.P. Souza, P.O. Patricio, F.C.C. Moura, New J. Chem. 39 (2015) 3051–3058.
[66] H.D. Oliveira, A.C. Silva, J.P. de Mesquita, F.V. Pereira, D.Q. Lima, J.D. Fabris, F.C.C. Moura, L.C.A. Oliveira, New J. Chem. 37 (2013) 2486–2491.
[67] A.S. Ganeshraja, K. Rajkumar, K.X. Zhu, X.N. Li, S. Thirumurugan, W. Xu, J. Zhang, M.H. Yang, K. Anbalagan, J.H. Wang, RSC Adv. 6 (2016) 72791–72802.
[68] M. Munoz, Z.M. de Pedro, J.A. Casas, J.J. Rodriguez, Appl. Catal. B 176 (2015) 249–265.
[69] A.D. Bokare, W. Choi, J. Hazard. Mater. 275 (2014) 121–135.
[70] P.V. Nidheesh, R. Gandhimathi, S.T. Ramesh, Environ. Sci. Pollut. Res. Int. 20 (2013) 2099–2132.
[71] E. Neyens, J. Baeyens, J. Hazard. Mater. 98 (2003) 33–50.
[72] G.P. Anipsitakis, D.D. Dionysiou, Environ. Sci. Technol. 37 (2003) 4790–4797.
[73] X.J. Yang, X.M. Xu, J. Xu, Y.F. Han, J. Am. Chem. Soc. 135 (2013) 16058–16061.
[74] G. Pliego, J.A. Zazo, P. Garcia-Munoz, M. Munoz, J.A. Casas, J.J. Rodriguez, Crit. Rev. Env. Sci. Tech. 45 (2015) 2611–2692.
[75] A.D. Purceno, A.P.C. Teixeira, A.B. Souza, J.D. Ardisson, J.P. de Mesquita, R.M. Lago, Appl. Clay Sci. 69 (2012) 87–92.
[76] Y. Wang, H. Wei, P. Liu, Y. Yu, Y. Zhao, X. Li, W. Jiang, J. Wang, X. Yang, C. Sun, Catal. Today 258 (2015) 120–131.
[77] X. Li, J. Wang, A.I. Rykov, V.K. Sharma, H. Wei, C. Jin, X. Liu, M. Li, S. Yu, C. Sun, D.D. Dionysiou, Catal. Sci. Technol. 5 (2015) 504–514.
[78] X. Li, J. Liu, A.I. Rykov, H. Han, C. Jin, X. Liu, J. Wang, Appl. Catal. B 179 (2015) 196–205.
[79] X. Li, A.I. Rykov, J. Wang, Catal. Commun. 77 (2016) 32–36.
[80] A.L. de Abreu, I.R. Guimaraes, A.D. Anastacio, M.C. Guerreiro, J. Mol. Catal. A: Chem. 356 (2012) 128–136.
[81] X. Li, A.I. Rykov, B. Zhang, Y. Zhang, J. Wang, Catal. Sci. Technol. 6 (2016) 7486–7494.
[82] X. Li, Z. Wang, B. Zhang, A.I. Rykov, M.A. Ahmed, J. Wang, Appl. Catal. B 181 (2016) 788–799.
[83] V.R. Stamenkovic, B. Fowler, B.S. Mun, G.F. Wang, P.N. Ross, C.A. Lucas, N.M. Markovic, Science 315 (2007) 493–497.
[84] A.A. Gewirth, M.S. Thorum, Inorg. Chem. 49 (2010) 3557–3566.
[85] R. Jasinski, Nature 201 (1964) 1212.
[86] S.L. Gojkovic, S. Gupta, R.F. Savinell, J. Electroanal. Chem. 462 (1999) 63–72.
[87] D. Scherson, A.A. Tanaka, S.L. Gupta, D. Tryk, C. Fierro, R. Holze, E.B. Yeager, R.P. Lattimer, Electrochim. Acta 31 (1986) 1247–1258.
[88] J.A.R. Vanveen, J.F. Vanbaar, K.J. Kroese, J. Chem. Soci.-Faraday Trans. I 77 (1981) 2827–2843.
[89] L. Ge, Y. Yang, L. Wang, W. Zhou, R. De Marco, Z. Chen, J. Zou, Z. Zhu, Carbon 82 (2015) 417–424.
[90] G. Faubert, G. Lalande, R. Cote, D. Guay, J.P. Dodelet, L.T. Weng, P. Bertrand, G. Denes, Electrochim. Acta 41 (1996) 1689–1701.
[91] G. Faubert, R. Cote, J.P. Dodelet, M. Lefevre, P. Bertrand, Electrochim. Acta 44 (1999) 2589–2603.
[92] U.I. Kramm, J. Herranz, N. Larouche, T.M. Arruda, M. Lefevre, F. Jaouen, P. Bogdanoff, S. Fiechter, I. Abs-Wurmbach, S. Mukerjee, J.P. Dodelet, Phys. Chem. Chem. Phys. 14 (2012) 11673–11688.
[93] Y.S. Zhu, B.S. Zhang, X. Liu, D.W. Wang, D.S. Su, Angew. Chem. Int. Ed. 53 (2014) 10673–10677.

[94] J.Y.C. Chen, L.N. Dang, H.F. Liang, W.L. Bi, J.B. Gerken, S. Jin, E.E. Alp, S.S. Stahl, J. Am. Chem. Soc. 137 (2015) 15090–15093.
[95] A. Zitolo, V. Goellner, V. Armel, M.T. Sougrati, T. Mineva, L. Stievano, E. Fonda, F. Jaouen, Nature Mater. 14 (2015) 937–942.
[96] F. Cheng, J. Shen, B. Peng, Y. Pan, Z. Tao, J. Chen, Nature Chem. 3 (2011) 79–84.
[97] E. Detsi, J.B. Cook, B.K. Lesel, C.L. Turner, Y.-L. Liang, S. Robbennolt, S.H. Tolbert, Energy Environ. Sci (2016) 540–549.
[98] X. Cui, P. Ren, D. Deng, J. Deng, X. Bao, Energy Environ. Sci (2016) 123–129.
[99] A. Hitihami-Mudiyanselage, M.P. Arachchige, T. Seda, G. Lawes, S.L. Brock, Chem. Mater. 27 (2015) 6592–6600.
[100] K. Weber, T. Kramer, H.S. Shafaat, T. Weyhermuller, E. Bill, M. van Gastel, F. Neese, W. Lubitz, J. Am. Chem. Soc. 134 (2012) 20745–20755.
[101] K. Zhu, M. Li, X. Li, X. Zhu, J. Wang, W. Yang, Chem. Commun. 52 (2016) 11803–11806.
[102] K. Zhu, H. Liu, M. Li, X. Li, J. Wang, X. Zhu, W. Yang, J. Mater. Chem. A 5 (2017) 7753–7758.
[103] Y. Su, D. Ao, H. Liu, Y. Wang, J. Mater. Chem. A 5 (2017) 8680–8689.
[104] Y. Liang, Y. Li, H. Wang, J. Zhou, J. Wang, T. Regier, H. Dai, Nature Mater. 10 (2011) 780–786.
[105] Q. Tang, L. Jiang, J. Liu, S. Wang, G. Sun, ACS Catal. 4 (2014) 457–463.
[106] X. Liu, Z. Chang, L. Luo, T. Xu, X. Lei, J. Liu, X. Sun, Chem. Mater. 26 (2014) 1889–1895.
[107] E. Lee, J.-H. Jang, Y.-U. Kwon, J. Power Sources 273 (2015) 735–741.
[108] X. Li, L. Yuan, J. Wang, L. Jiang, A.I. Rykov, D.L. Nagy, C. Bogdan, M.A. Ahmed, K. Zhu, G. Sun, W. Yang, Nanoscale 8 (2016) 2333–2342.
[109] M. Armand, J.M. Tarascon, Nature 451 (2008) 652–657.
[110] J.M. Tarascon, M. Armand, Nature 414 (2001) 359–367.
[111] H. Ahouari, G. Rousse, J. Rodriguez-Carvajal, M.-T. Sougrati, M. Saubanere, M. Courty, N. Recham, J.-M. Tarascon, Chem. Mater. 27 (2015) 1631–1639.
[112] R. Chen, R. Heinzmann, S. Mangold, V.S.K. Chakravadhanula, H. Hahn, S. Indris, J. Phys. Chem. C 117 (2013) 884–893.
[113] M. Chamas, M.-T. Sougrati, C. Reibel, P.-E. Lippens, Chem. Mater. 25 (2013) 2410–2420.
[114] L. Tao, G. Rousse, J.N. Chotard, L. Dupont, S. Bruyere, D. Hanzel, G. Mali, R. Dominko, S. Levasseur, C. Masquelier, J. Mater. Chem. A 2 (2014) 2060–2070.
[115] S. Ferrari, M.C. Mozzati, M. Lantieri, G. Spina, D. Capsoni, M. Bini, Sci. Rep. 6 (2016) 27896–27907.
[116] H.Y. Asl, P. Stanley, K. Ghosh, A. Choudhury, Chem. Mater. 27 (2015) 7058–7069.
[117] C. Vidal-Abarca, P. Lavela, M.J. Aragon, N. Plylahan, J.L. Tirado, J. Mater. Chem. 22 (2012) 21602–21607.
[118] N. Kiziltas-Yavuz, M. Yavuz, S. Indris, N.N. Bramnik, M. Knapp, O. Dolotko, B. Das, H. Ehrenberg, A. Bhaskar, J. Power Sources 327 (2016) 507–518.
[119] G. Oyama, S.-i Nishimura, M. Chung, A. Yamada, Electrochemistry 82 (2014) 855–858.
[120] J. Zhao, L. Zhao, N. Dimov, S. Okada, T. Nishida, J. Electrochem. Soc. 160 (2013) A3077–A3081.
[121] S. Novikova, S. Yaroslavtsev, V. Rusakov, A. Chekannikov, T. Kulova, A. Skundin, A. Yaroslavtsev, J. Power Sources 300 (2015) 444–452.
[122] L. de Biasi, G. Lieser, C. Drager, S. Indris, J. Rana, G. Schumacher, R. Monig, H. Ehrenberg, J.R. Binder, H. Gesswein, J. Power Sources 362 (2017) 192–201.
[123] R.Y. Chen, R. Witte, R. Heinzmann, S.H. Ren, S. Mangold, H. Hahn, R. Hempelmann, H. Ehrenberg, S. Indris, Phys. Chem. Chem. Phys. 18 (2016) 7695–7701.
[124] G. Lieser, C. Drager, L. de Biasi, S. Indris, H. Gesswein, S. Glatthaar, M.J. Hoffmann, H. Ehrenberg, J.R. Binder, J. Power Sources 274 (2015) 1200–1207.
[125] K. Xu, B. Sun, J. Lin, W. Wen, Y. Pei, S. Yan, M. Qiao, X. Zhang, B. Zong, Nat. Commun. 5 (2014) 5783–5790.
[126] A.K. Padhi, K.S. Nanjundaswamy, J.B. Goodenough, J. Electrochem. Soc. 144 (1997) 1188–1194.
[127] A.R. Armstrong, N. Kuganathan, M.S. Islam, P.G. Bruce, J. Am. Chem. Soc. 133 (2011) 13031–13035.
[128] M.S. Islam, R. Dominko, C. Masquelier, C. Sirisopanaporn, A.R. Armstrong, P.G. Bruce, J. Mater. Chem. 21 (2011) 9811–9818.
[129] K. Kravchyk, L. Protesescu, M.I. Bodnarchuk, F. Krumeich, M. Yarema, M. Walter, C. Guntlin, M.V. Kovalenko, J. Am. Chem. Soc. 135 (2013) 4199–4202.
[130] J.A. Brant, D.M. Massi, N.A.W. Holzwarth, J.H. MacNeil, A.P. Douvalis, T. Bakas, S.W. Martin, M.D. Gross, J.A. Aitken, Chem. Mater. 27 (2015) 189–196.
[131] A.Y. Khodakov, W. Chu, P. Fongarland, Chem. Rev. 107 (2007) 1692–1744.
[132] V.R. Calderone, N.R. Shiju, D. Curulla-Ferre, S. Chambrey, A. Khodakov, A. Rose, J. Thiessen, A. Jess, G. Rothenberg, Angew. Chem. Int. Ed. 52 (2013) 4397–4401.
[133] H.M.T. Galvis, J.H. Bitter, C.B. Khare, M. Ruitenbeek, A.I. Dugulan, K.P. de Jong, Science 335 (2012) 835–838.
[134] G.B. Yu, B. Sun, Y. Pei, S.H. Xie, S.R. Yan, M.H. Qiao, K.N. Fan, X.X. Zhang, B.N. Zong, J. Am. Chem. Soc. 132 (2010) 935–937.
[135] E. de Smit, B.M. Weckhuysen, Chem. Soc. Rev. 37 (2008) 2758–2781.
[136] D.B. Bukur, K. Okabe, M.P. Rosynek, C.P. Li, D.J. Wang, K. Rao, G.P. Huffman, J. Catal. 155 (1995) 353–365.
[137] R.P. Mogorosi, N. Fischer, M. Claeys, E. van Steen, J. Catal. 289 (2012) 140–150.
[138] W. Ma, G. Jacobs, D.E. Sparks, V.R.R. Pendyala, S.G. Hopps, G.A. Thomas, H.H. Hamdeh, A. MacLennan, Y. Hu, B.H. Davis, J. Catal. 326 (2015) 149–160.
[139] M.K. Gnanamani, G. Jacobs, H.H. Hamdeh, W.D. Shafer, B.H. Davis, Catal. Today 207 (2013) 50–56.
[140] K. Lazar, Hyperfine Interact. 217 (2013) 57–65.
[141] I. Perez De Berti, J. Bengoa, N. Fellenz, R. Mercader, S. Marchetti, Rev. Sci. Instrum. 86 (2015) 1–5.
[142] J.T. Lim, C.S. Kim, D.H. Chun, J.C. Park, J. Korean Phys. Soc. 68 (2016) 302–305.
[143] H.J. Zhang, H.F. Ma, H.T. Zhang, W.Y. Ying, D.Y. Fang, Catal. Lett. 142 (2012) 131–137.
[144] Z.H. Chonco, A. Ferreira, L. Lodya, M. Claeys, E. van Steen, J. Catal. 307 (2013) 283–294.
[145] J.M. Cho, S.R. Lee, J. Sun, N. Tsubaki, E.J. Jang, J.W. Bae, ACS Catal. 7 (2017) 5955–5964.
[146] V.P. Santos, L. Borges, S. Sartipi, B. van der Linden, A.I. Dugulan, A. Chojecki, T. Davidian, M. Ruitenbeek, G.R. Meima, F. Kapteijn, M. Makkee, J. Gascon, Appl. Catal. A- Gen. 533 (2017) 38–48.
[147] G.W. Huber, S. Iborra, A. Corma, Chem. Rev. 106 (2006) 4044–4098.
[148] D.M. Alonso, S.G. Wettstein, J.A. Dumesic, Chem. Soc. Rev. 41 (2012) 8075–8098.
[149] M. Besson, P. Gallezot, C. Pinel, Chem. Rev. 114 (2014) 1827–1870.
[150] I.L.C. Buurmans, B.M. Weckhuysen, Nat. Chem. 4 (2012) 873–886.
[151] P.Y. Dapsens, C. Mondelli, J. Perez-Ramirez, Chem. Soc. Rev. 44 (2015) 7025–7043.
[152] A. Corma, L.T. Nemeth, M. Renz, S. Valencia, Nature 412 (2001) 423–425.
[153] M.S. Holm, S. Saravanamurugan, E. Taarning, Science 328 (2010) 602–605.
[154] P. Wolf, M. Valla, A.J. Rossini, A. Comas-Vives, F. Núñez-Zarur, B. Malaman, A. Lesage, L. Emsley, C. Copéret, I. Hermans, Angew. Chem. Int. Ed. 53 (2014) 10179–10183.
[155] J. Dijkmans, M. Dusselier, W. Janssens, M. Trekels, A. Vantomme, E. Breynaert, C. Kirschhock, B.F. Sels, ACS Catal. 6 (2016) 31–46.
[156] Z. Xiao, S. Jin, X. Wang, W. Li, J. Wang, C. Liang, J. Mater. Chem. 22 (2012) 16598–16605.
[157] N. Ji, T. Zhang, M. Zheng, A. Wang, H. Wang, X. Wang, J.G. Chen, Angew. Chem. Int. Ed. 47 (2008) 8510–8513.
[158] A. Wang, T. Zhang, Acc. Chem. Res. 46 (2013) 1377–1386.
[159] J. Pang, M. Zheng, R. Sun, A. Wang, X. Wang, T. Zhang, Green Chem. 18 (2015) 342–359.
[160] R. Sun, M. Zheng, J. Pang, X. Liu, J. Wang, X. Pan, A. Wang, X. Wang, T. Zhang, ACS Catal. 6 (2016) 191–201.
[161] R.N. Olcese, M. Bettahar, D. Petitjean, B. Malaman, F. Giovanella, A. Dufour, Appl. Catal. B Environ. 115–116 (2012) 63–73.
[162] C. Opris, B. Cojocaru, N. Gheorghe, M. Tudorache, S.M. Coman, V.I. Parvulescu, B. Duraki, F. Krumeich, J.A. van Bokhoven, J. Catal. 339 (2016) 209–227.
[163] M. Virginie, J. Adánez, C. Courson, L.F. de Diego, F. García-Labiano, D. Niznansky, A. Kiennemann, P. Gayán, A. Abad, Appl. Catal. B Environ. 121–122 (2012) 214–222.
[164] J. Yang, S. Li, L. Zhang, X. Liu, J. Wang, X. Pan, N. Li, A. Wang, Y. Cong, X. Wang, T. Zhang, Appl. Catal. B Environ. 201 (2017) 266–277.
[165] X. Chen, J. Wang, K. Yang, C. Meng, C.T. Williams, C. Liang, J. Phys. Chem. C 119 (2015) 29052–29061.
[166] V. Goelden, S. Sokolov, V.A. Kondratenko, E.V. Kondratenko, Appl. Catal. B 101 (2010) 130–136.
[167] Z. Sobalik, E. Tabor, J. Novakova, N.K. Sathu, K. Zaveta, J. Catal. 289 (2012) 164–170.
[168] P. Boron, L. Chmielarz, J. Gurgul, K. Latka, B. Gil, J.-M. Krafft, S. Dzwigaj, Catal. Today 235 (2014) 210–225.
[169] A. Boubnov, A. Roppertz, M.D. Kundrat, S. Mangold, B. Reznik, C.R. Jacob, S. Kureti, J.D. Grunwaldt, Appl. Surf. Sci. 386 (2016) 234–246.
[170] Y. Wu, C. Cordier, E. Berrier, N. Nuns, C. Dujardin, P. Granger, Appl. Catal. B 140 (2013) 151–163.
[171] T.J. Vulic, A.F.K. Reitzmann, K. Lazar, J. Chem Eng, 207 (2012) 913–922.
[172] M. Tian, X.D. Wang, T. Zhang, Catal. Sci. Technol. 6 (2016) 1984–2004.
[173] P.F. Xie, Y.J. Luo, Z. Ma, C.Y. Huang, C.X. Miao, Y.H. Yue, W.M. Hua, Z. Gao, J. Catal. 330 (2015) 311–322.
[174] P. Boron, L. Chmielarz, J. Gurgul, K. Latka, B. Gil, B. Marszalek, S. Dzwigaj, Microporous Mesoporous Mater. 203 (2015) 73–85.
[175] P. Sazama, N.K. Sathu, E. Tabor, B. Wichterlova, S. Sklenak, Z. Sobalik, J. Catal. 299 (2013) 188–203.
[176] P. Boron, L. Chmielarz, J. Gurgul, K. Latka, T. Shishido, J.M. Krafft, S. Dzwigaj, Appl. Catal. B 138 (2013) 434–445.
[177] J. Wang, H. Xia, X. Ju, Z. Feng, F. Fan, C. Li, J. Catal. 300 (2013) 251–259.
[178] P.F. Xie, Z. Ma, T. Meng, C.Y. Huang, C.X. Miao, Y.H. Yue, W.M. Hua, Z. Gao, J. Mol. Catal. A: Chem. 409 (2015) 50–58.
[179] S. Zhu, X. Wang, A. Wang, Y. Cong, T. Zhang, Chem. Commun. (2007) 1695–1697.
[180] S. Zhu, X. Wang, A. Wang, T. Zhang, Catal. Today 131 (2008) 339–346.
[181] Y. Zhu, X. Wang, Y. Huang, Y. Zhang, G. Wu, J. Wang, T. Zhang, J. Phys. Chem. C 116 (2012) 24487–24495.
[182] Y. Zhu, X. Wang, Y. Zhang, J. Wang, Y. Huang, C. Kappenstein, T. Zhang, Appl. Catal. A- Gen. 409 (2011) 194–201.
[183] Y. Zhang, X. Wang, Y. Zhu, T. Zhang, Appl. Catal. B 129 (2013) 382–393.
[184] Y. Zhu, X. Wang, G. Wu, Y. Huang, Y. Zhang, J. Wang, T. Zhang, J. Phys. Chem. C 116 (2012) 671–680.
[185] Y. Zhang, X.D. Wang, Y.Y. Zhu, X. Liu, T. Zhang, J. Phys. Chem. C 118 (2014) 10792–10804.
[186] Y. Zhang, X.D. Wang, Y.Y. Zhu, B.L. Hou, X.F. Yang, X. Liu, J.H. Wang, J. Li, T. Zhang, J. Phys. Chem. C 118 (2014) 1999–2010.